Supplementary Information for

# Host-Guest Molecular Interaction Promoted Urea Electrosynthesis over Precisely Designed Conductive Metal-Organic Frameworks

Menglei Yuan [#1,2], Junwu Chen [#1,2], Honghua Zhang [1,2], Qiongguang Li [1,2], Le Zhou [1,2], Chao Yang [1,2,3], Rongji Liu [1,2,4], Zhanjun Liu [2,5], Suojiang Zhang [1,2*], Guangjin Zhang [1,2,3*]

[1] CAS Key Laboratory of Green Process Engineering, State Key Laboratory of Multiphase Complex Systems, Institute of Process Engineering, Chinese Academy of Sciences, Beijing, 100190, China

[2] School of Chemical Engineering, Center of Materials Science and Optoeletronics Engineering, University of Chinese Academy of Sciences, Beijing, 100049, China

[3] Chemistry and Chemical Engineering Guangdong Laboratory, Shantou, 515031, China

[4] Iorganic Chemistry I, Ulm University, Ulm, 89081, Germany

[5] CAS Key Laboratory of Carbon Materials, Institute of Coal Chemistry, Chinese Academy of Sciences, 030001, Taiyuan, China

[*] Correspondence: zhanggj@ipe.ac.cn; sjzhang@ipe.ac.cn

## Methods

### Materials

Cobalt sulfate heptahydrate [$CoSO_4 \cdot 7H_2O$, 99.99%], 2-methylbenzimidazole [2-mbIM, $C_8H_8N_2$, 98%], pyromellitic dianhydride [PMDA, $C_{10}H_2O_6$, 99%], tetrahydrofuran [THF, $C_4H_8O$], phosphoric acid [$H_3PO_4$, ≥ 85%], sulfuric acid [$H_2SO_4$, ≥ 85%], iron chloride [$FeCl_3$, 99.9%], diacetylmonoxime [$C_4H_7NO_2$, AR], thiosemicarbazide [$CH_5N_3S$, 99%] and potassium bicarbonate [$KHCO_3$, ≥ 99.99%] were purchased from Sigma-Aldrich Chemical Reagent Co., Ltd. Water were purified by Millipore system and ethanol was utilized without further purification.

### Preparation of Co-PMDA-2-mbIM

1.68 mmol $CoSO_4 \cdot 7H_2O$ was first dissolved in 30 mL THF. Subsequently, 3.39 mmol 2-mbIM and 0.60 mmol PMDA were dispersed in 10 mL THF and the obtained solution were slowly dripped into the aforementioned metal salt solution. The mixed solution was sonicated for 10 min to obtain a homogeneous solution and transferred to a 50 mL hydrothermal autoclave at 95 ℃ for 48 h. The resulting product was washed several times with methanol and DI and dried in the oven at 60 ℃ for 24 h.

### Preparation of Co-PMDA

The preparation procedure of Co-PMDA was similar to that of Co-PMDA-2-mbIM, except that 2-mbIM ligand wasn't added.

### Characterization

X-ray diffraction (XRD, X'PERT PRO MPD diffractometer, Cu Kα radiation, λ=0.15418 nm, scanned range of 2-90°) was used to identify the crystal structure of all prepared catalysts. Scanning electron microscopy (SEM, JSM-7800F Prime) and transmission electron microscopy (TEM, JEM-2100F) were utilized to investigate the morphology of all samples. The Raman measurements were carried out on a Renishaw Raman Test system (λ=532 nm). Nitrogen and carbon dioxide temperature programmed desorption (TPD) were recorded on the AutoChem II2920. X-ray photoelectron spectroscopy (XPS) data were collected by using Krato, AXIS-HS monochromatized Al Kα cathode source of 75-150 W under ultrahigh vacuum.

Fourier Transform Infrared Spectrometer (FTIR) and the spin state of the catalysts were tested on NICOLET Is 50 (Thermo) and MPMS-3 (Quantum Design), respectively. Moreover, the UV-visible adsorption spectra were recorded on a spectrophotometer (UV-2550). H NMR spectra were collected on a superconducting-magnet NMR spectrometer (Bruker AVANCE III HD 700 MHz).

**Crystal structure characterization of Co-PMDA-2-mbIM**

Single-crystal XRD data was collected on a Bruker Smart Apex-II CCD diffractometer. The Co-PMDA-2-mbIM was tested at the monochromatic Mo-Kα radiation (λ=0.71073 Å) equipped with ω-scan technique.

**Electrochemical measurements**

All electrochemical characterizations were performed using a CHI 660E workstation coupled with a three-electrode system in a two-compartment cell separated by Nafion 211 membrane. And the Nafion membrane was heated in $H_2O_2$ (5%) aqueous solution at 80 ℃ for 1 h, heating in 0.1 M $H_2SO_4$ at 80 ℃ for 1 h and then treating by boiling in ultrapure water for another 1 h, respectively. Carbon cloth utilized in this work was purchased from CeTech (W1S1009 type) and treated with the mixture of $H_2SO_4$:$H_2O_2$ (1:3 vol.) for 12 h to remove surface impurities. To avoid contamination with nitrogen-containing species in the air, electrodes were used either immediately after preparation or kept in a vacuum before being used in electrochemical experiments. The prepared catalyst loaded on a piece of pretreated carbon cloth (1×3 $cm^2$) was used as the working electrode, a graphite rod, and Ag/AgCl (saturated KCl electrolyte) were employed as counter electrode and reference electrode, respectively. Potential without iR-compensated were converted to RHE scale via the following equation: E (vs. RHE) = E (vs. Ag/AgCl) + 0.0591 × pH + 0.197 (pH = 6.8 in $CO_2$-saturated electrolyte and $N_2$ + $CO_2$-saturated electrolyte in 0.1 M $KHCO_3$; pH = 8.3 for $N_2$-saturated electrolyte in 0.1 M $KHCO_3$). The catalyst ink for the working electrode was prepared by dispersing 3.59 mg of catalyst in a mixed solution of 30 μL Nafion (0.5 wt%), 500 μL ethanol, and 470 μL water followed by sonication for 30 minutes. Mass loading of 0.3 mg $cm^{-2}$ was used for the electrochemical study. All experiments were carried out at room temperature (25 ℃). To remove the impurities in the inlet

gas, such as $NO_X$, the pre-purification of high-purity $N_2$ (purity 99.999%) and $CO_2$ (purity 99.99%) by passing through a saturator filled with 0.05 M NaOH and a saturator filled with 0.05 M $H_2SO_4$ solution to remove any possible contaminants. Before carrying out all the electrochemical characterizations, the 0.1 M $KHCO_3$ electrolyte solution was purged with $CO_2$ + $N_2$ for 30 minutes. Cyclic voltammetry (CV) test was carried out at a scan rate of 50 mV $s^{-1}$ ranging from 0-0.2 V (vs. RHE). Linear sweep voltammetry (LSV) was also conducted at a scan rate of 5 mV $s^{-1}$. Chronoamperometric tests were then conducted at different potentials and $CO_2$ + $N_2$ was continuously fed into the cathodic cell during the experiments. The recycle test was to perform five consecutive cycles of chronoamperometric runs without changing the electrolyte at -0.5 V vs. RHE. Electrochemical impedance spectroscopy (EIS) was conducted at a frequency range from 100 kHz to 1 Hz with a 10 mV AC signal amplitude at -0.5 V vs. RHE on a PAR-STAT 2273 test system.

**Determination of urea concentration by diacetyl monoxime method**

The urea concentration was determined by the diacetyl monoxime method [*Clin Chim Acta* 1980, **107**(1)**:** 3-9]. 5g of diacetylmonoxime (DAMO) and 100 mg of thiosemicarbazide (TSC) were dissolved in distilled water and diluted to 1000 mL, denoted as DAMO-TSC solution. Then, 100 mL concentrated phosphoric acid was mixed with 300 mL of concentrated sulfuric acid and 600 mL distilled water, then 100 mg $FeCl_3$ was dissolved in the above solution, denoted as the acid-ferric solution. Typically, 1 mL of the sample solution was removed from the cathodic chamber. Afterward, 1 mL of DAMO-TSC solution and 2 mL of acid-ferric solution were added into 1 ml of sample solution. Next, the mixed solution was heated to 100 ℃ and maintained at this temperature for 15 min. When the solution cooled to 25 ℃, the UV-Vis absorption spectrum was collected at a wavelength of 525 nm. The concentration-absorbance curve was calibrated using standard urea solution for a series of concentrations. The fitting curve shows good linear relation of absorbance value with urea concentration by three times independent calibration tests.

**Calculation of Faradaic efficiency (FE) and urea formation rate**

The FE for urea electrosynthesis was defined as the amount of electric charge used for

producing urea divided by the total charge passed through the electrodes during the electrolysis. Assuming six electrons were needed to produce one urea molecule, the FE was calculated according to the following equation:

$$FE = 6 \times F \times C_{urea} \times V / (60.06 \times Q)$$

The rate of formation of urea was calculated using the following equation:

$$\text{urea yield rate} = C_{urea} \times V / (m_{cat} \times t \times 60.06)$$

Where F is Faraday constant (96485 C $mol^{-1}$), $C_{urea}$ is the measured mass concentration of urea; V is the volume of the cathodic reaction electrolyte; Q is the quantity of applied charge/electricity; t is the time for which the potential was applied; m is the mass of catalyst loaded at the carbon cloth.

**Determination of $NH_3$ concentration by indophenol blue method**

When tested in 0.1 M $KHCO_3$, the produced $NH_3$ was spectrophotometrically determined by the indophenol blue method [*Nat Mater* 2013, **12**(9)**:** 836-841]. Typically, 2 mL of the sample solution was removed from the cathodic chamber. Afterward, 2 mL of 1.0 M NaOH solution containing 5 wt% salicylic acid and 5 wt% sodium citrate was added, followed by 1 mL NaClO solution (0.05 M) and 0.2 mL of an aqueous solution of sodium nitroferricyanide (1 wt%) were added. After standing at room temperature for 2 hours, the UV-Vis absorption spectrum was collected at a wavelength of 655 nm. The concentration-absorbance curve was calibrated using standard $NH_4Cl$ solution for a series of concentrations. The fitting curve shows good linear relation of absorbance value with $NH_4Cl$ concentration by three times independent calibration tests. The 8 μL of different concentration of $^{15}NH_4^+$ (0.05 – 0.35 ppm) mixed with 0.5 mL of DMSO-$d_6$ and 8 μL of maleic acid ($C_4H_4O_4$) was quantified by $^1H$ NMR (700 MHz). The corresponding standard curve can be determined as $y = 18.854x + 0.003$ ($R^2 = 0.997$).

**Calculation of Faradaic efficiency (FE) and $NH_3$ formation rate**

The FE for NRR was defined as the amount of electric charge used for producing $NH_3$ divided by the total charge passed through the electrodes during the electrolysis. Assuming three electrons were needed to produce one $NH_3$ molecule, the FE was calculated according to the following equation:

$$FE = 3 \times 0.318 \times F \times C_{NH4Cl} \times V / (17 \times Q)$$

The rate of formation of NH3 was calculated using the following equation:

$$NH_3 \text{ yield rate} = 0.318 \times C_{NH4Cl} \times V / (m_{cat} \times t \times 53.5)$$

Where F is Faraday constant (96485 C $mol^{-1}$), $C_{NH4Cl}$ is the measured mass concentration of $NH_4Cl$; V is the volume of the cathodic reaction electrolyte; Q is the quantity of applied charge/electricity; t is the time for which the potential was applied; $m_{cat}$ is the mass of catalyst loaded at the carbon cloth.

**Calculation of $e_g$ filling**

The total effective magnetic moments ($\mu_{eff}$) samples could be evaluated from M-T data by using the Equation (1), according to the Langevin theory:

$$\mu_{eff} = \sqrt{8C}\mu_B \qquad (1)$$

Where C is Curies constant and obtained from the fittings on the susceptibility ($\chi$=M/H) above the paramagnetic transition temperatures by a Curie-Weiss law $\chi$=C/(T-$\Theta$), where $\Theta$ is Curie Weiss temperature.

$V_{HS}$ and $V_{LS}$ are the volume fractions for $Co^{3+}$ and $Co^{4+}$ in HS and LS states, respectively, which can be determined by Equation (3) and (4):

$$\mu_{eff} = g\sqrt{S_{HS}(S_{HS}+1)V_{HS} + S_{LS}(S_{LS}+1)V_{LS}} \qquad (2)$$

$$V_{HS} + V_{LS} = 1 \qquad (3)$$

As for Co-PMDA-2-mbIM ($Co^{4+}$), where the Lande factor g = 2.5, $S_{HS}$ = 2.5 and $S_{LS}$ = 0; as for Co-PMDA ($Co^{3+}$), where the Lande factor g = 2, $S_{HS}$ = 2 and $S_{LS}$ = 0.

When we obtained $V_{HS}$ and $V_{LS}$ values, consequently, the $e_g$ filling (x) can be further calculated by Equation (4):

$$x = V_{HS} \times S_{HS} \qquad (4)$$

The obtained $V_{HS}$, $V_{LS}$ values and the calculated $e_g$ filling are shown in Table S2.

**DFT calculations**

Spin-polarized density functional theory (DFT) calculations were conducted using the Vienna ab initio simulation package (VASP) [*Physical Review B* 1996, **54**(16)**:** 11169-11186]. The projector augmented wave (PAW) method was used to describe electron-ion interactions. A generalized gradient approximation (GGA) to the

exchange-correlation functional of Perdew–Burke–Ernzernhof (PBE) with DFT+U correction (U − J = 3.32 eV for Co 3d) was applied [*Physical Review B* 1992, **45**(23)**:** 13244-13249; *Phys Rev Lett* 1996, **77**(18)**:** 3865-3868]. Gaussian smearing of 0.05 eV was applied. The cutoff energy for the plane-wave basis set was set as 520 eV, and the total energy convergence was set to be lower than $2 \times 10^{-6}$ eV, with the force convergence set at 0.02 eV/Å for geometric optimizations. A Monkhorst-Pack k-points setting of 4 × 3 × 2 and 6 × 4 × 4 was used to sample the Brillouin zone for geometry optimizations and electronic structure computations, respectively. The DFT-D3 empirical correction method was employed to describe van der Waals interactions [*The Journal of Chemical Physics* 2010, **132**(15)**:** 154104]. Specifically, the implicit solvation model of VASPsol has been employed to describe the effect of electrostatics, cavitation and dispersion on the interaction between a solute and solvent. The free energy of the electrochemical steps of the reaction was calculated based on the computational hydrogen electrode (CHE) model. The free energies of species were calculated as $G = E_{DFT} + E_{ZPE} - T\Delta S$, where $E_{DFT}$ was obtained from DFT energy, $E_{ZPE,}$ and $T\Delta S$ of adsorbed species were calculated by vibration analysis, whereas the thermodynamic corrections for gas molecules were from the standard database.

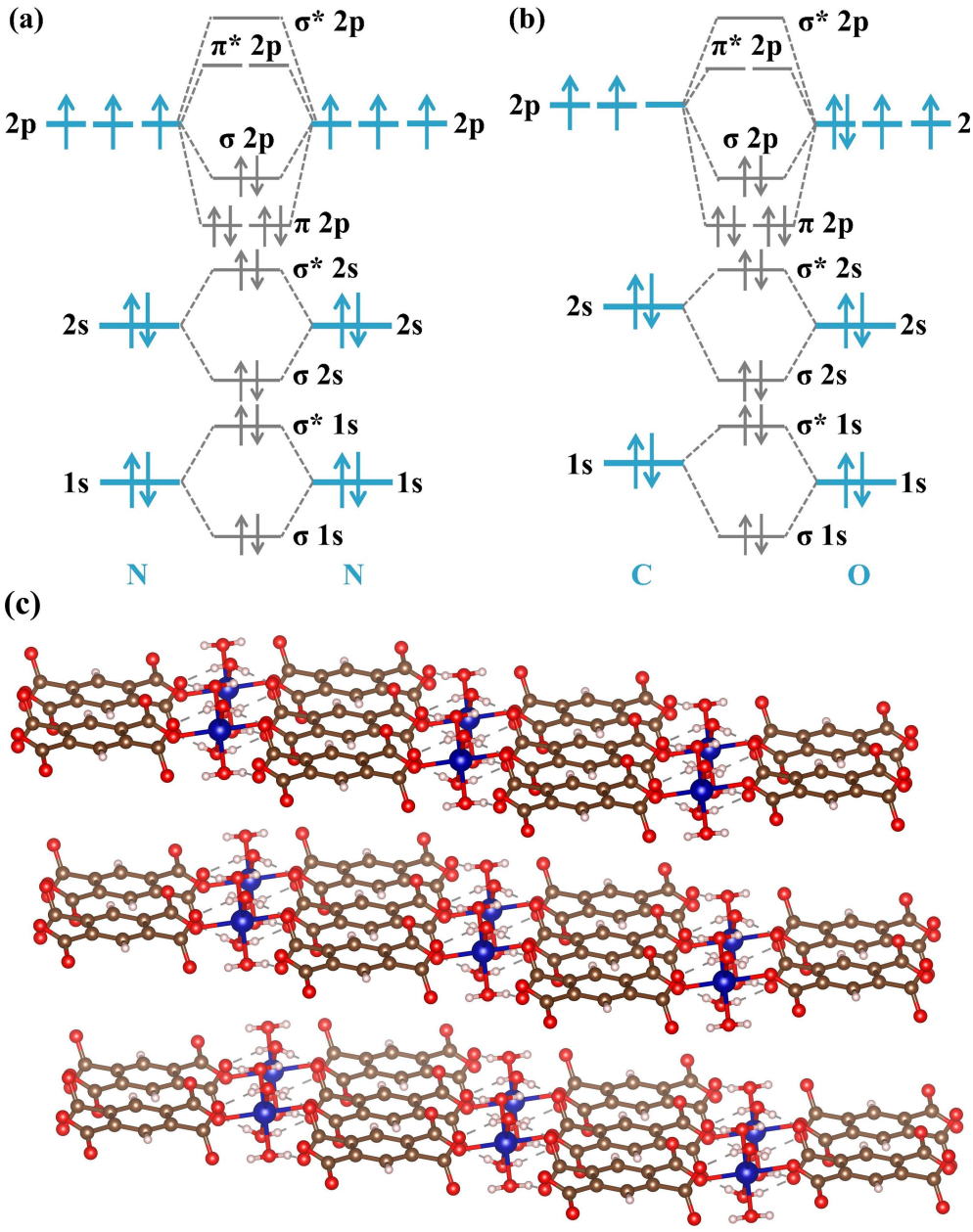


**Fig. S1 |** The molecular orbitals of (a) *$N_2$ and (b) *CO intermediates. (c) The crystal structure of Co-PMDA.

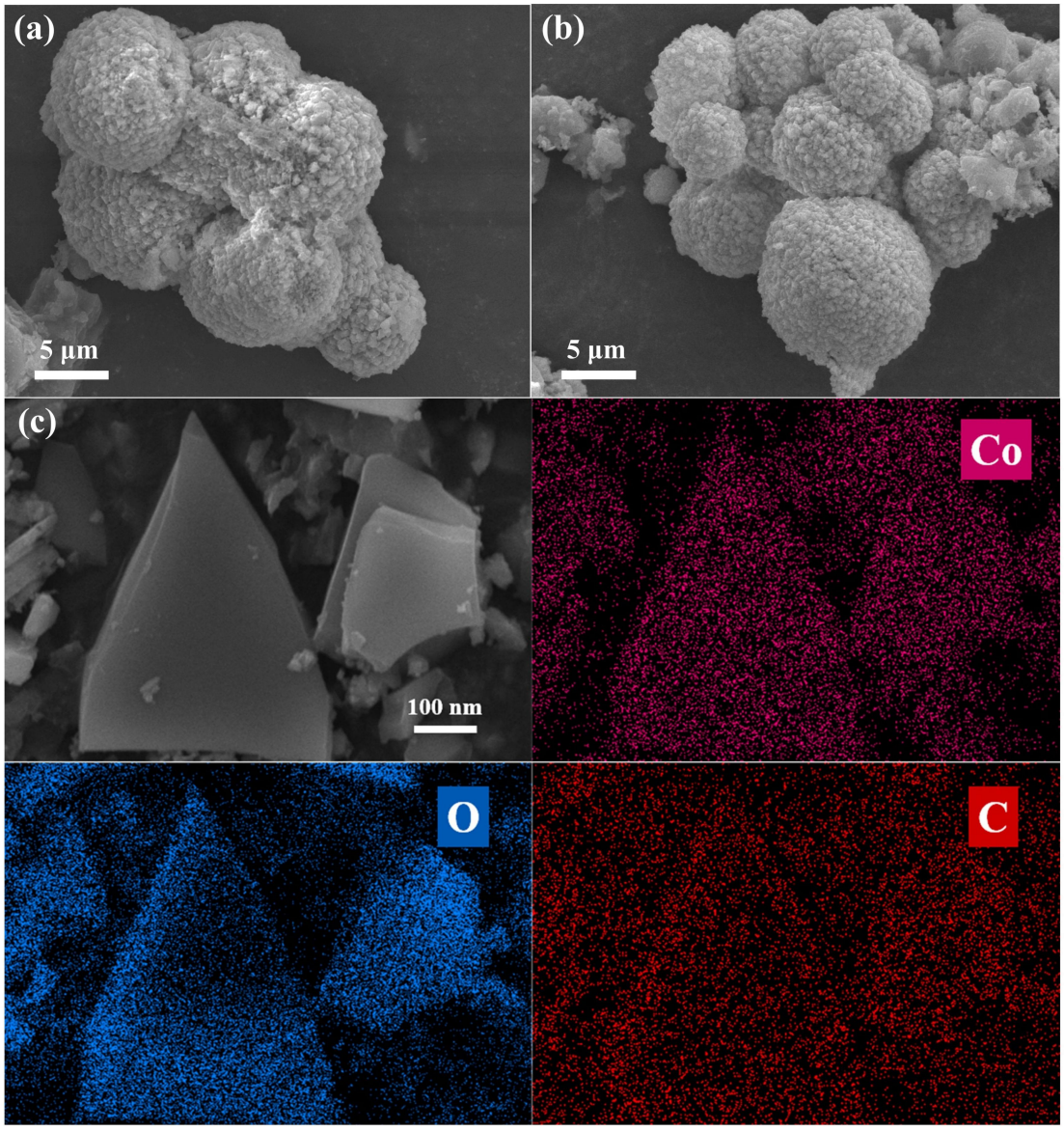


**Fig. S2** | (a-b) The SEM image of Co-PMDA-2-mbIM; (c) the SEM image and the corresponding elemental mapping of Co-PMDA catalyst.

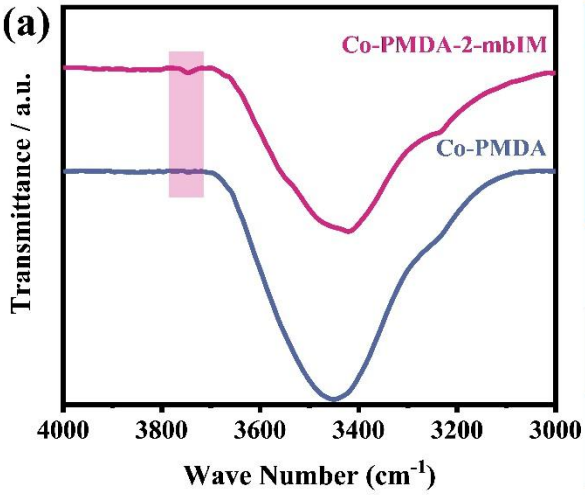


| (b) | Co-PMDA | Co-PMDA-2-mbIM |
|---|---|---|
| C | 3.1655 | 2.9401 |
| θ (K) | 3.35 | -21.94 |
| $\mu_{eff}$ ($\mu_B$) | 5.03 | 4.77 |

**Fig. S3** | (a) The FTIR spectrum and (b) the corresponding Curie constant C, Weiss constant θ and effective paramagnetic moment $\mu_{eff}$ of Co-PMDA and Co-PMDA-2-mbIM catalysts.

**(a)**

湖南省华中特种气体有限公司

地址：湖南省衡南县花桥镇 114 号　网址：WWW.CCSG.CN

电话：0734-8755678　传真:0734-8123618

氮气-$^{15}N_2$ 分析报告

产品名称：气态氮-$^{15}N_2$

CAS 号：29817-79-6

规　格：99%N-15（atom）

数　量：5L/瓶*1

LOT 号：15N3612

箱　号：4261

| 项　目 | 检测标准 | 检测结果 |
|---|---|---|
| 外　观 | 无色气体 | |
| 丰　度 | 99% | 99.13% 15N; 0.87% 14N |

上述产品经检验质量合格，准予出厂。

质检员：麦丽冰　　复核员：

**(b)** Hunan Central China Special Gas Co., Ltd

Nitrogen-$^{15}N_2$ Analysis Report

Product Name: Gaseous N-$^{15}N_2$

CAS Number: 29817-79-6

Specifications: 99%N-15 (atom)

Quantity: 5L/bottle * 1

LOT Number: 15N3612

Case Number: 4261

| Project | Test Standard | Test Result |
|---|---|---|
| Appearance | Colorless Gas | |
| Purity | 99% | 99.13% 15N; 0.87% 14N |

The above products have passed the inspection and are allowed to leave the factory

Quality inspector: Libing Mai　　Reviewer: Chen

**(c)**

| Supplier | Purity | CoA | Batch Number | Purified Method | Purified Time | Flow Rate |
|---|---|---|---|---|---|---|
| Central China Special Gas Co. Ltd | 99.13% 15N; 0.87% 14N | Above picture | 15N3612 | 0.05 M $H_2SO_4$; 0.05 M NaOH | 12h | $N_2$ (30 sccm); $CO_2$ (30 sccm) |

**Fig. S4 |** The certificate of analysis (CoA) of (a) commercial $^{15}N_2$ (original) and (b) in English; (c) the detailed information of commercial $^{15}N_2$.

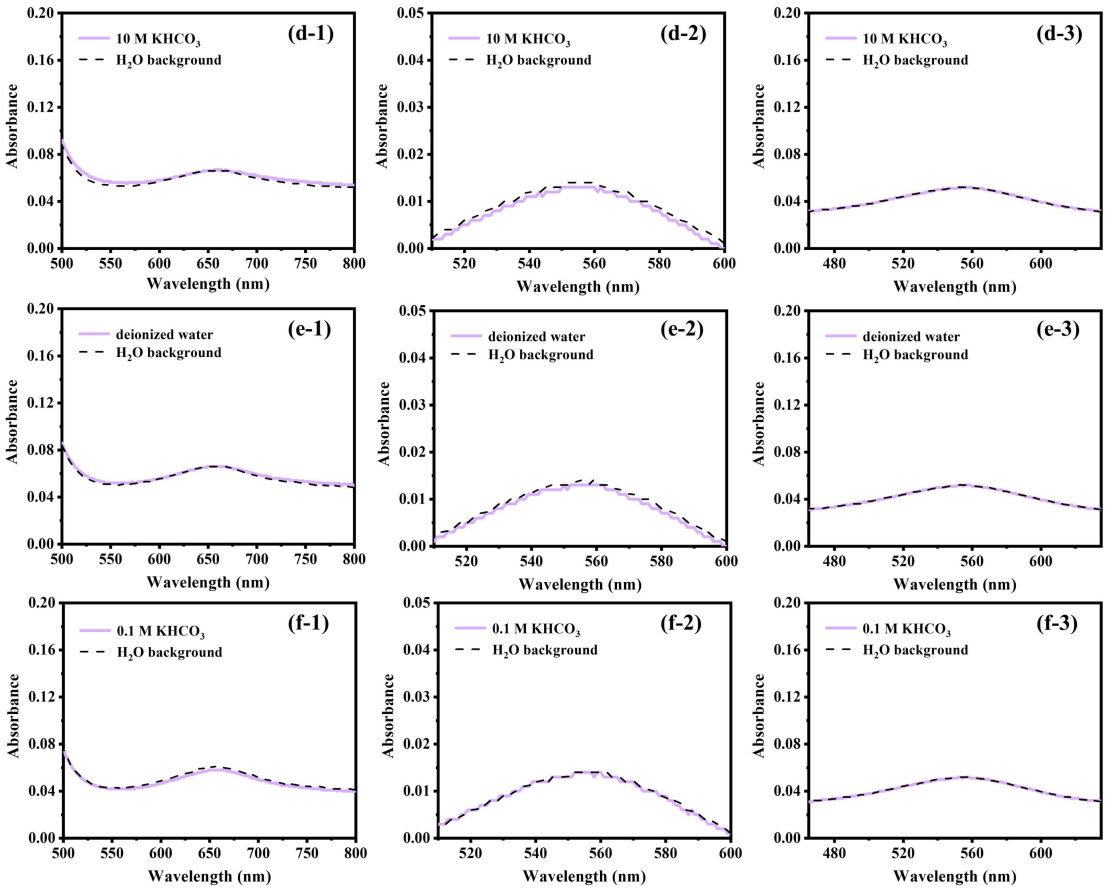


**Fig. S4 |** The UV-Vis absorption spectra of the (d) 10 M $KHCO_3$ solution, (e) deionized water and (f) 0.1 M $KHCO_3$ solution treated by (d-1, e-1, f-1) indophenol blue method for $NH_3$ analysis, (d-2, e-2, f-2) Griess tests for $NO_2^-$ analysis, (d-3, e-3, f-3) modified Griess tests for $NO_3^-$ analysis.

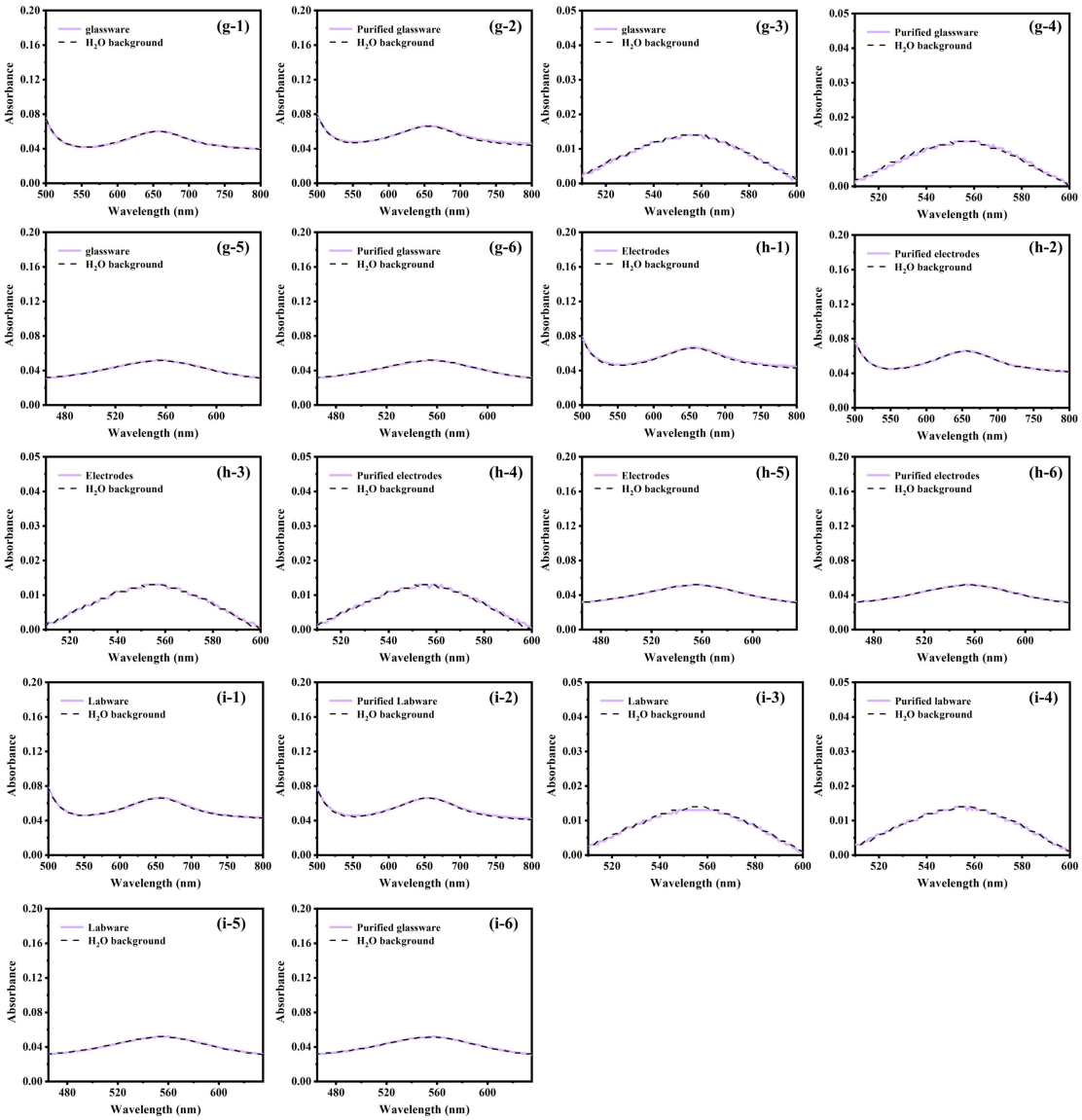


**Fig. S4 |** The UV-Vis absorption spectra of the (g) glassware and purified glassware, (h) electrodes and purified electrodes and (i) labware and purified labware treated by (g-1, g-2, h-1, h-2, i-1, i-2) indophenol blue method for $NH_3$ analysis, (g-3, g-4, h-3, h-4, i-3, i-4) Griess tests for $NO_2^-$ analysis, (g-5, g-6, h-5, h-6, i-5, i-6) modified Griess tests for $NO_3^-$ analysis.

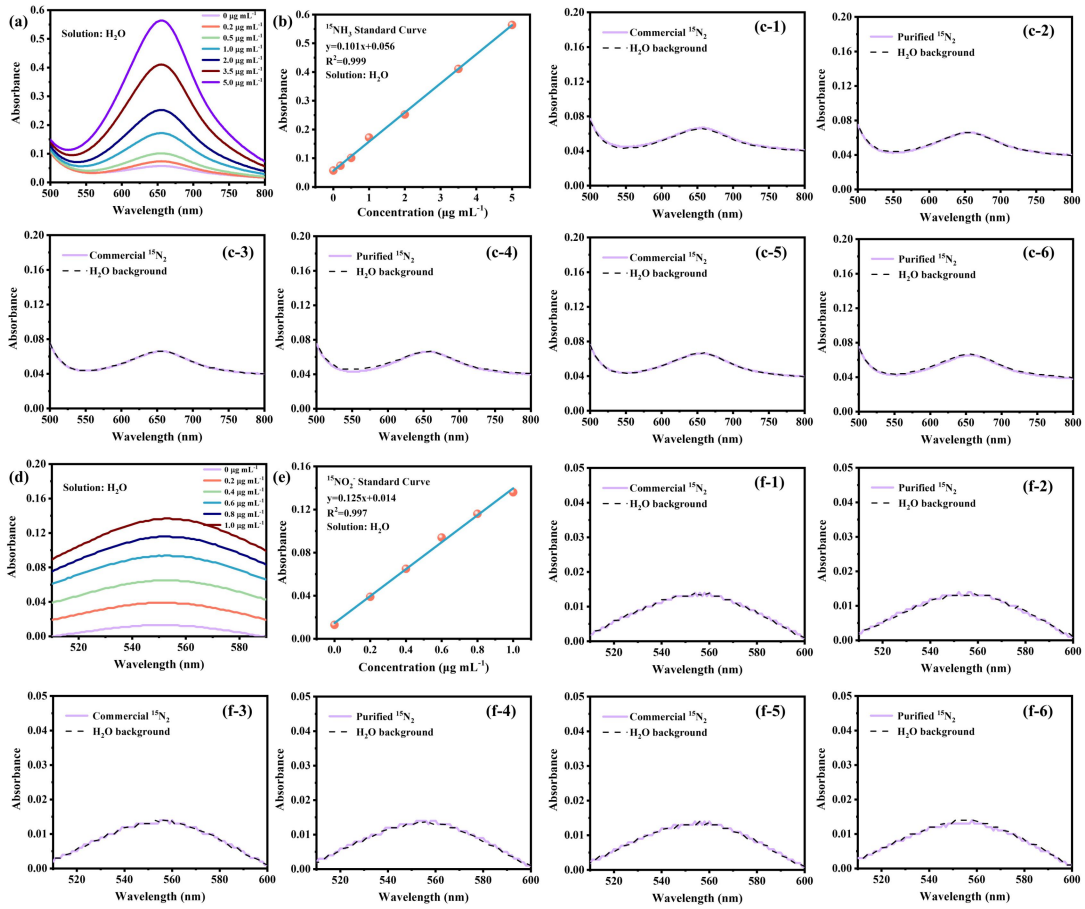


**Fig. S5 |** The UV-Vis absorption spectra of the deionized water treated by commercial $^{15}N_2$ and purified $^{15}N_2$ using (a-c) indophenol blue method for $^{15}NH_3$ analysis, (d-f) Griess tests for $^{15}NO_2^-$ analysis.

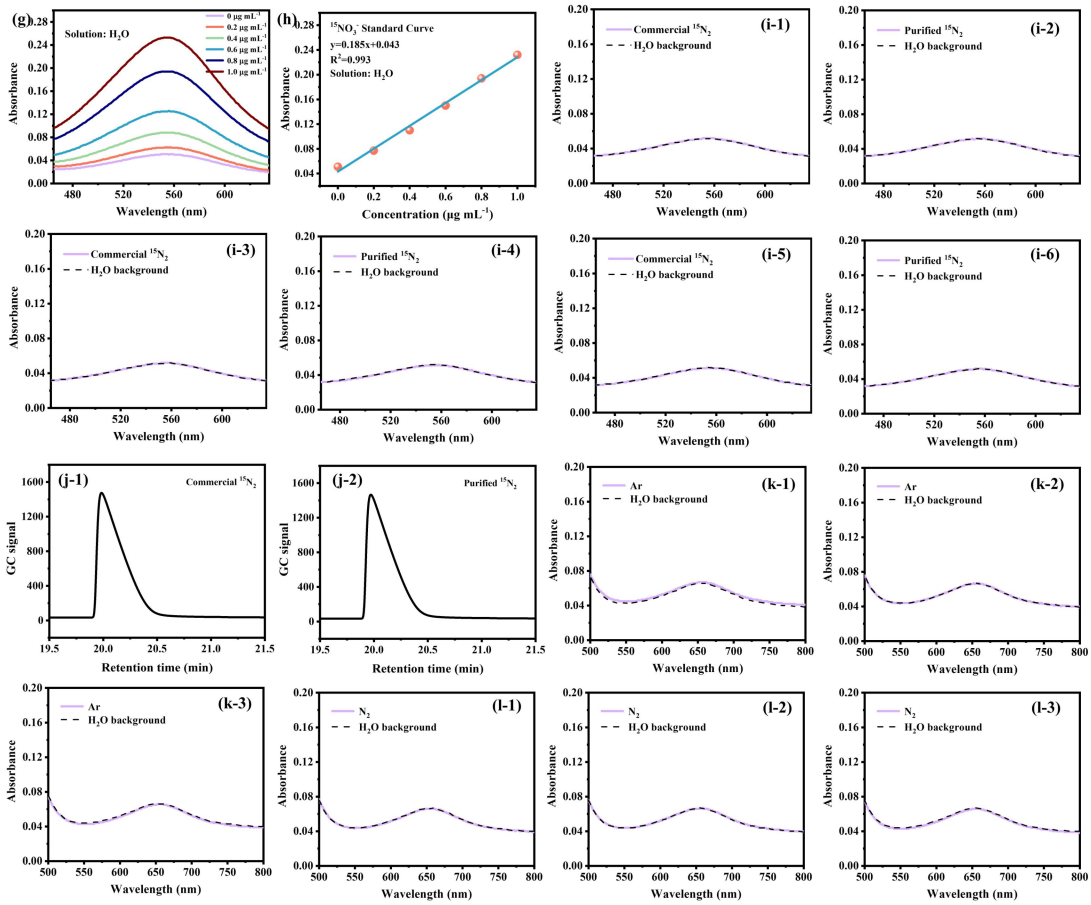


**Fig. S5 |** The UV-Vis absorption spectra of the deionized water treated by commercial $^{15}N_2$ and purified $^{15}N_2$ using (g-i) modified Griess tests for $^{15}NO_3^-$ analysis. (j) Gas chromatography (GC) spectra of commercial $^{15}N_2$ and purified $^{15}N_2$. The UV-Vis absorption spectra of the electrolyte solution that electrolysis under (k) Ar and (l) $N_2$ without any applied potential for three times.

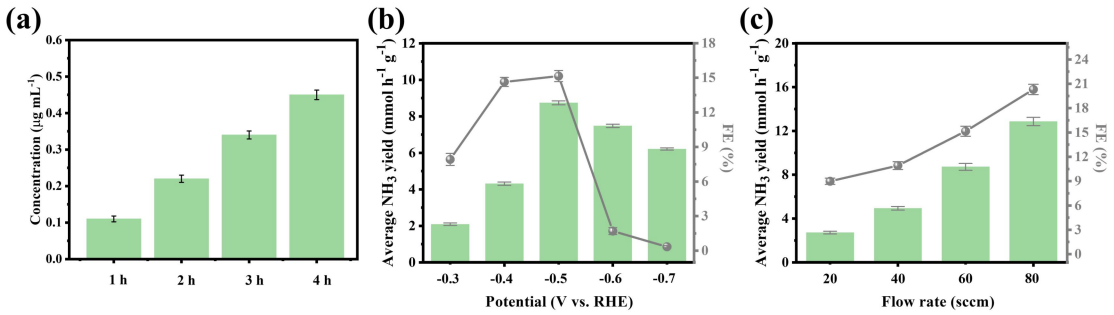


**Fig. S6 |** (a) The concentration of $^{15}NH_3$ at different time-point. The $^{15}NH_3$ yield rate and Faradaic efficiency of Co-PMDA-2-mbIM catalyst catalyzed at (b) different electrolytic potentials and (c) different flow rate.

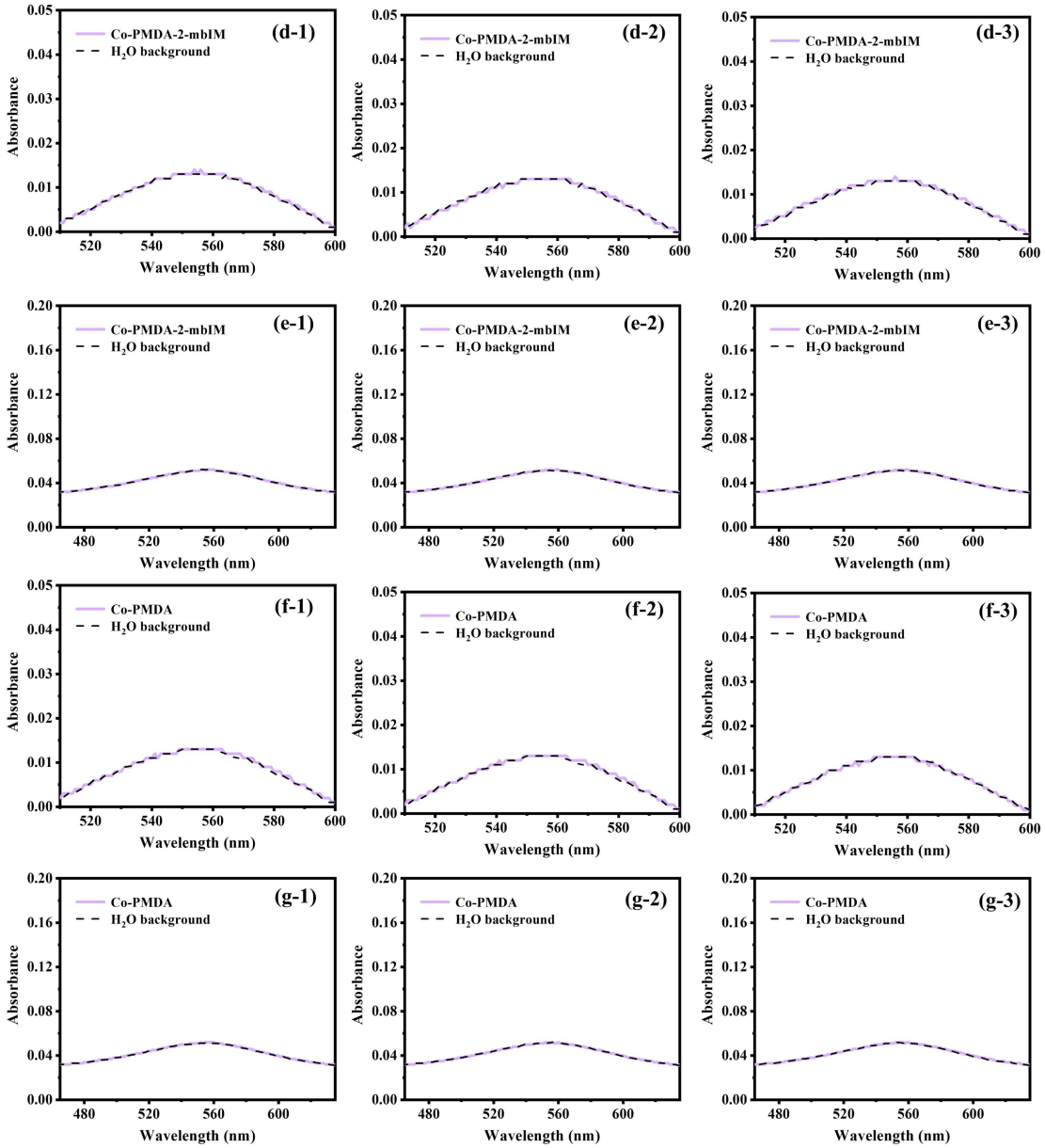


**Fig. S6 |** The detection of the amount of $NO_x$ of the (d-e) Co-PMDA-2-mbIM and (f-g) Co-PMDA samples present in the electrochemical cell at the optimal potential (-0.5 V vs. RHE) electrolysis under $^{14}N_2$. The UV-Vis absorption spectra of the solution treated by (d-1, d-2, d-3, f-1, f-2, f-3) Griess tests for $NO_2^-$ analysis, (e-1, e-2, e-3, g-1, g-2, g-3) modified Griess tests for $NO_3^-$ analysis.

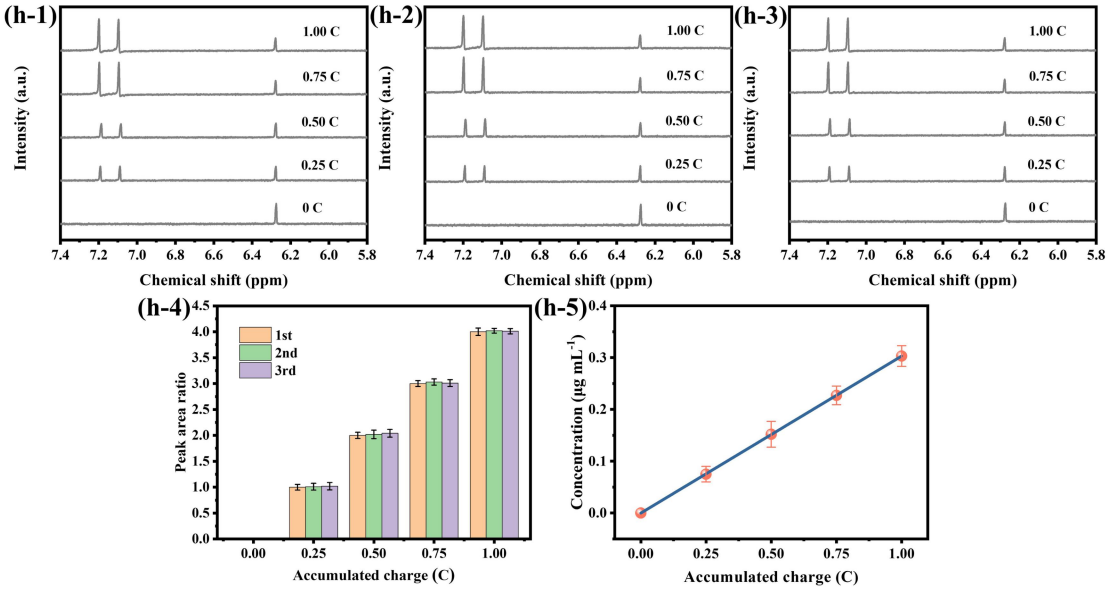


**Fig. S6** | (h-1~h-3) $^{1}H$ NMR spectra of $^{15}NH_3$ from all three $^{15}N_2$ reduction experiments (electrolysis at -0.4 V vs. RHE) as a function of charge passed. (h-4) The integral area ratio ($^{15}NH_3$ / $C_4H_4O_4$) from all three independent tests as a function of charge passed. (h-5) The average concentration of $^{15}NH_3$ as measured by NMR from the $^{15}N_2$ reduction experiments as a function of charge passed.

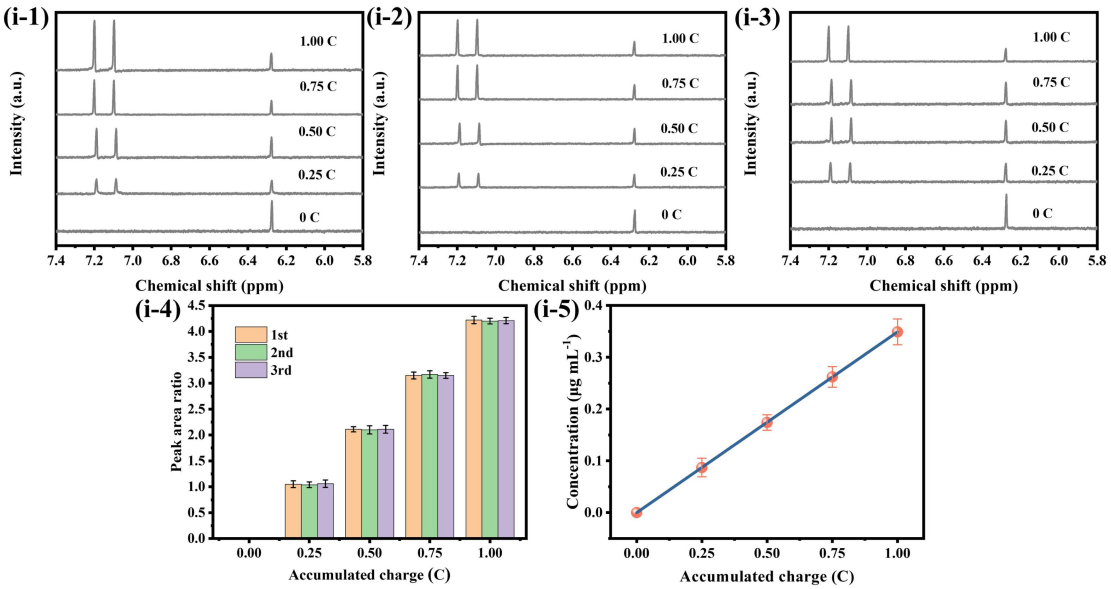


**Fig. S6 |** (i-1~i-3) $^{1}H$ NMR spectra of $^{15}NH_3$ from all three $^{15}N_2$ reduction experiments (electrolysis at -0.5 V vs. RHE) as a function of charge passed. (i-4) The integral area ratio ($^{15}NH_3$ / $C_4H_4O_4$) from all three independent tests as a function of charge passed. (i-5) The average concentration of $^{15}NH_3$ as measured by NMR from the $^{15}N_2$ reduction experiments as a function of charge passed.

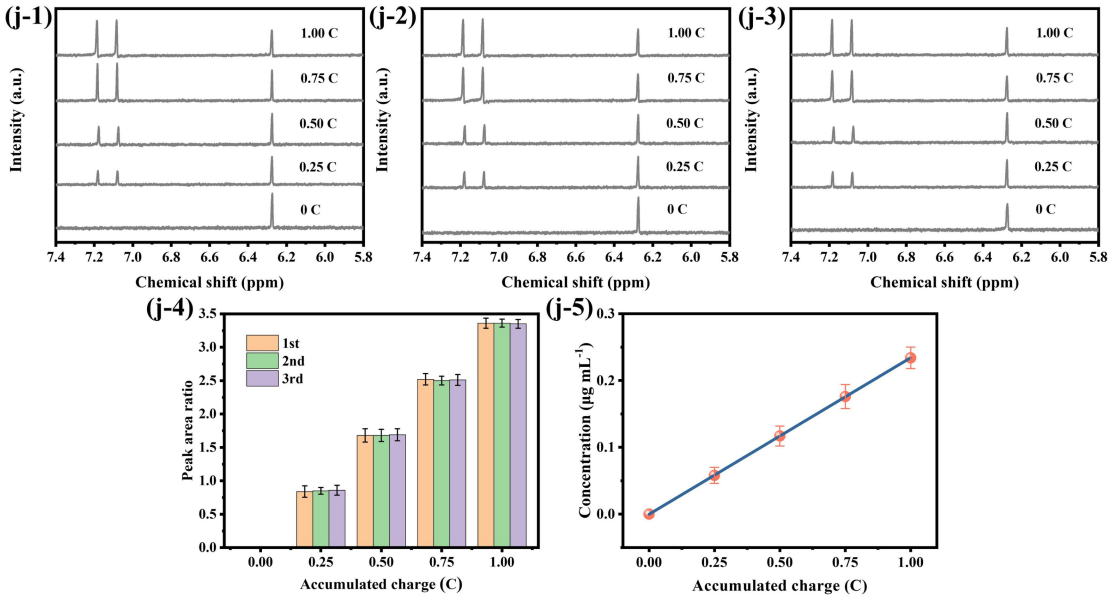


**Fig. S6 |** (j-1~j-3) $^{1}H$ NMR spectra of $^{15}NH_3$ from all three $^{15}N_2$ reduction experiments (electrolysis at -0.6 V vs. RHE) as a function of charge passed. (j-4) The integral area ratio ($^{15}NH_3$ / $C_4H_4O_4$) from all three independent tests as a function of charge passed. (j-5) The average concentration of $^{15}NH_3$ as measured by NMR from the $^{15}N_2$ reduction experiments as a function of charge passed.

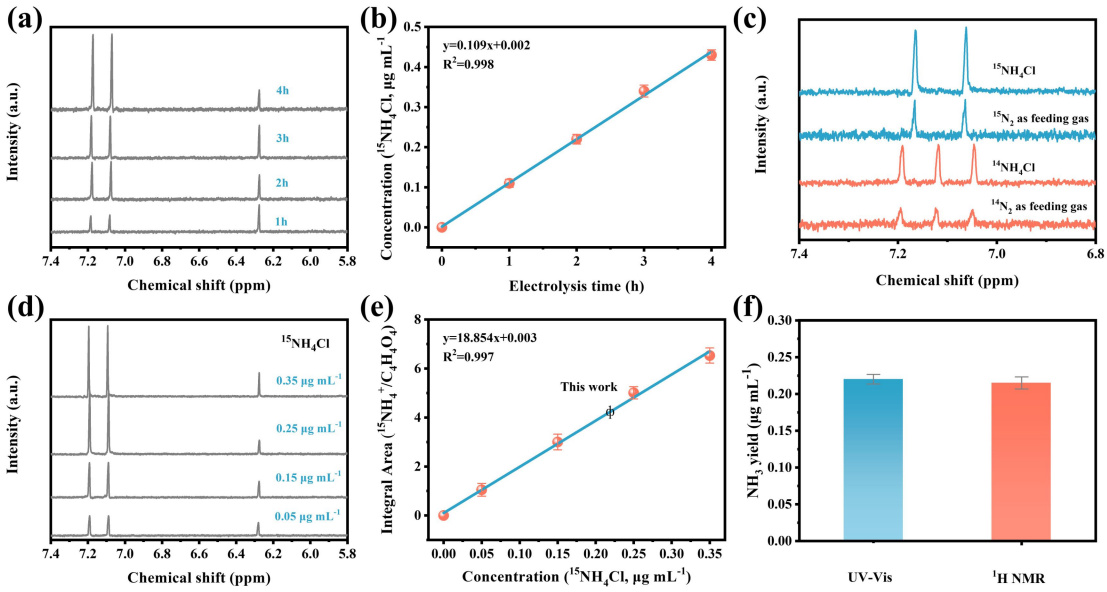


**Fig. S7 |** (a) $^{1}H$ NMR spectra of $^{15}NH_3$ product catalyzed at different electrolysis time and (b) the related electrolysis time - concentration linear relation; (c) $^{1}H$ NMR spectra of the electrolytes using $^{15}N_2$ and $^{14}N_2$ as the feeding gas; (d) $^{1}H$ NMR spectra of standard $^{15}NH_4Cl$ solution with various concentrations of 0.05-0.35 μg $mL^{-1}$; (e) integral area ($^{15}NH_4Cl$ / $C_4H_4O_4$) - concentration linear relation calibrated using standard $^{15}NH_4Cl$ solution; (f) the $^{15}NH_3$ yield of Co-PMDA-2-mbIM catalyst after 2h electrolysis detected by UV-Vis and $^{1}H$ NMR spectroscopy.

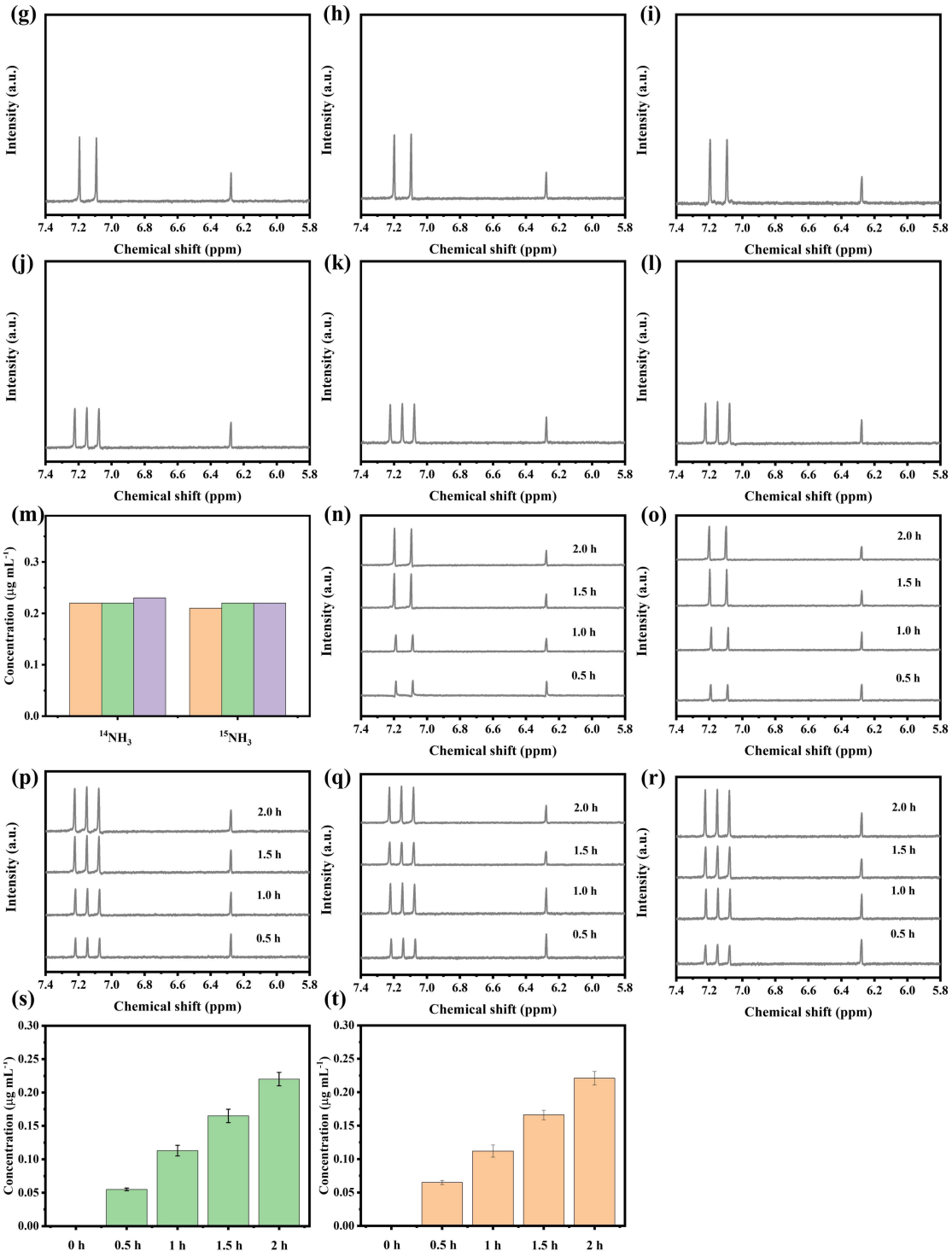


**Fig. S7 |** The $^{1}H$ NMR spectra of (g-i) $^{15}NH_3$ and (j-l) $^{14}NH_3$ catalyzed at -0.5 V vs. RHE by the Co-PMDA-2-mbIM catalyst; (m) The quantitative agreement of the concentration of $^{15}NH_3$ and $^{14}NH_3$. The $^{1}H$ NMR spectra of (n-o) $^{15}N_2$ and (p-r) $^{14}N_2$ catalyzed at different time-point. The concentration of (s) $^{15}NH_3$ and (t) $^{14}NH_3$ at different time-point.

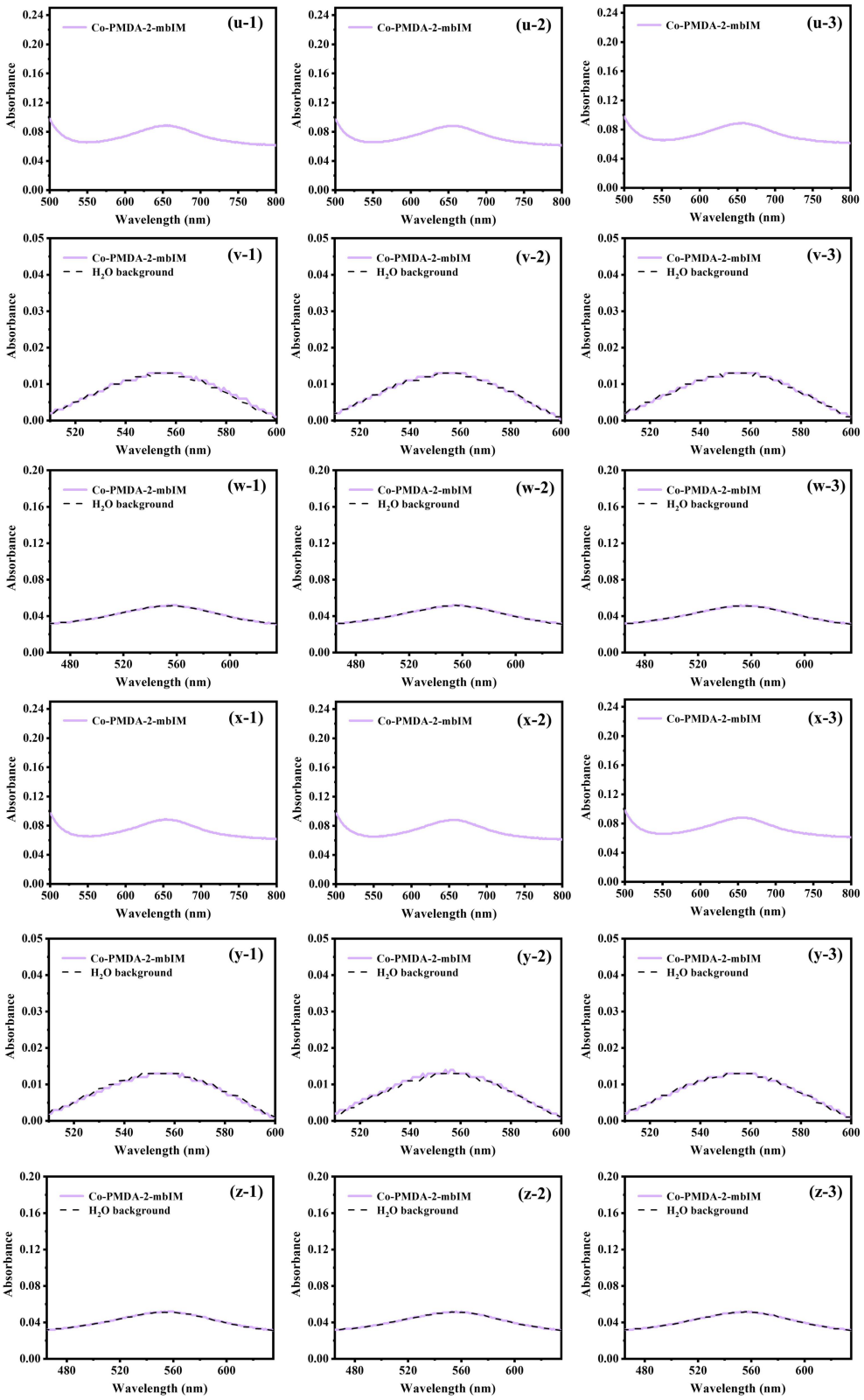


**Fig. S7** | The UV-Vis absorption spectra the (u) $^{14}NH_3$, (v) $^{14}NO_2^-$, (w) $^{14}NO_3^-$, (x) $^{15}NH_3$, (y) $^{15}NO_2^-$ and (z) $^{15}NO_3^-$ catalyzed by the Co-PMDA-2-mbIM catalysts with a small and fixed volume of $^{14}N_2$ and $^{15}N_2$ gas.

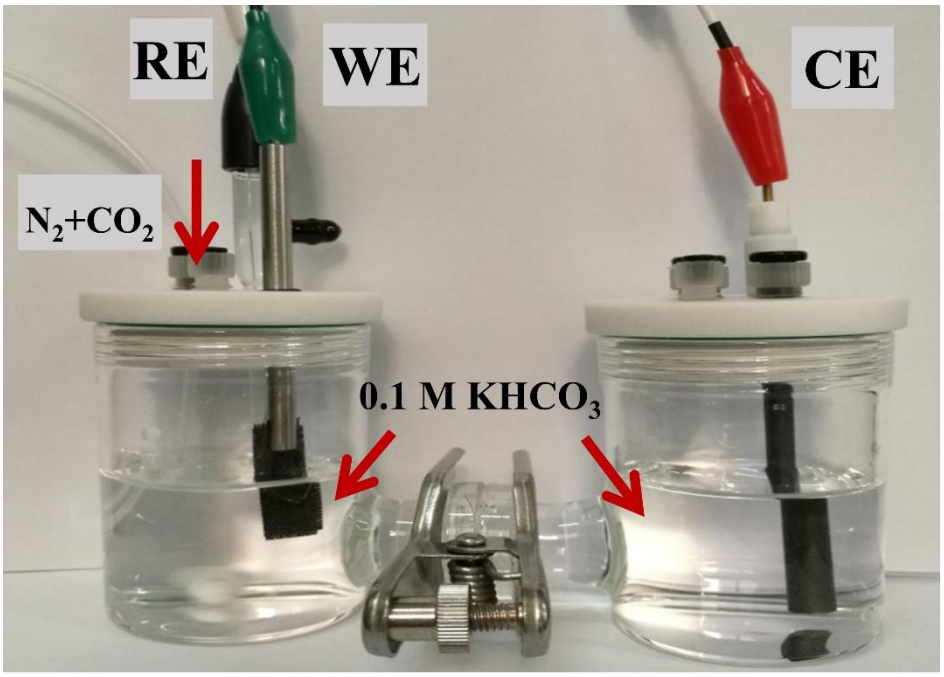


**Fig. S8 |** The optical photograph of the H-type cell for urea electrosynthesis testing.

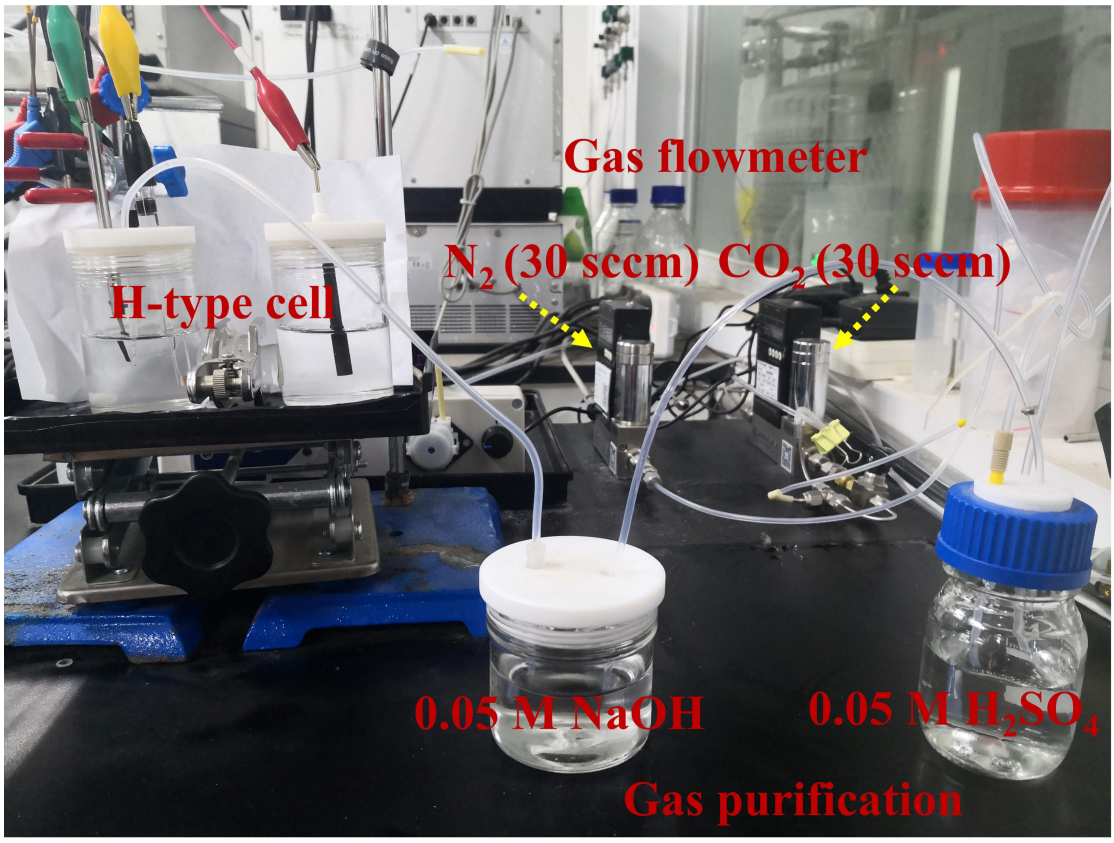


**Flow rate:** $N_2$ (30 sccm); $CO_2$ (30 sccm)
**Purification time:** 12 h
**Purification agents:** 0.05 M NaOH; 0.05 M $H_2SO_4$

**Fig. S9 |** The optical photograph of detailed experimental set-up for both $N_2$ and $CO_2$ gas purification. Noteworthy that this experimental set-up is also suitable for NRR test. The operation procedure of NRR experiment is similar with the above, we only need to turn off the switch of the flow meter for controlling $CO_2$ and the flow rate of $N_2$ can be determined as 30 sccm during NRR test.

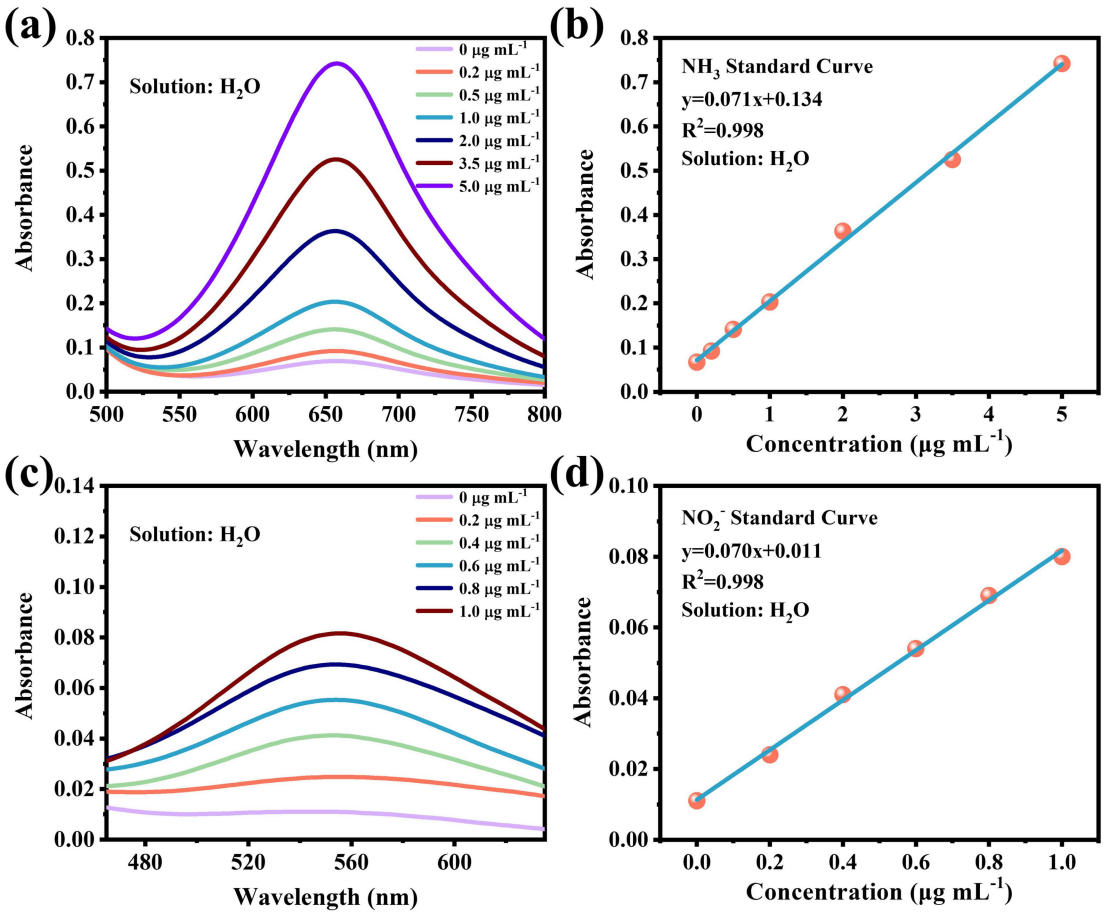


**Fig. S10** | The calibration curves for (a-b) the colorimetric $^{14}NH_3$ assay using the indophenol blue method and (c-d) the colorimetric NOx assay using the N-(-1-naphthyl)-ethylenediamine dihydrochloride spectrophotometric method in deionized water.

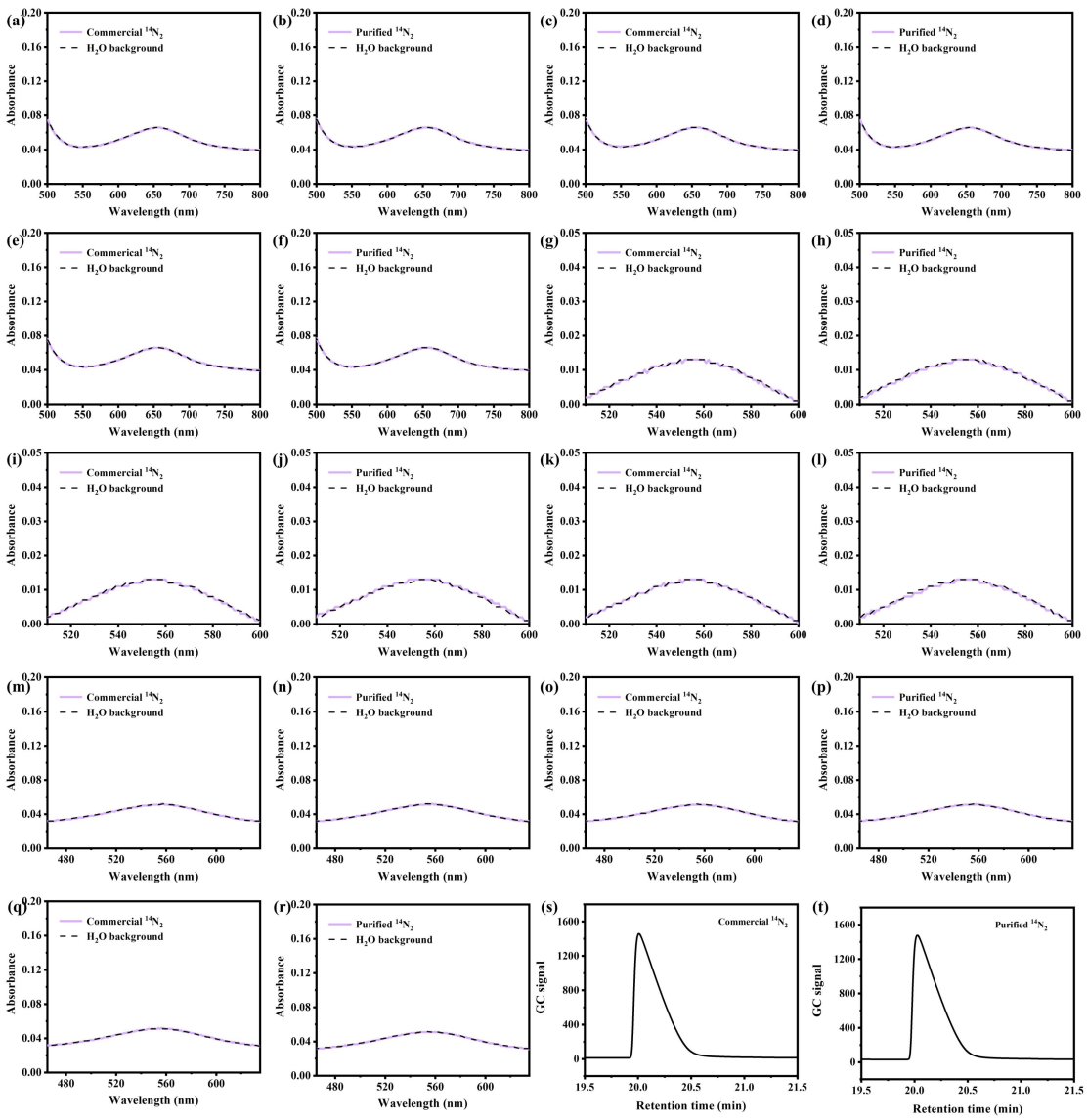


**Fig. S11 |** The UV-Vis absorption spectra of the deionized water treated by (a, c, e) commercial $^{14}N_2$ and (b, d, f) purified $^{14}N_2$ using indophenol blue method, (g, i, k) commercial $^{14}N_2$ and (h, j, l) purified $^{14}N_2$ with Griess tests for $NO_2^-$ analysis, (m, o, q) commercial $^{14}N_2$ and (n, p, r) purified $^{14}N_2$ with modified Griess tests for $NO_3^-$ analysis. (s, t) Gas chromatography (GC) spectra of commercial $^{14}N_2$ and purified $^{14}N_2$.

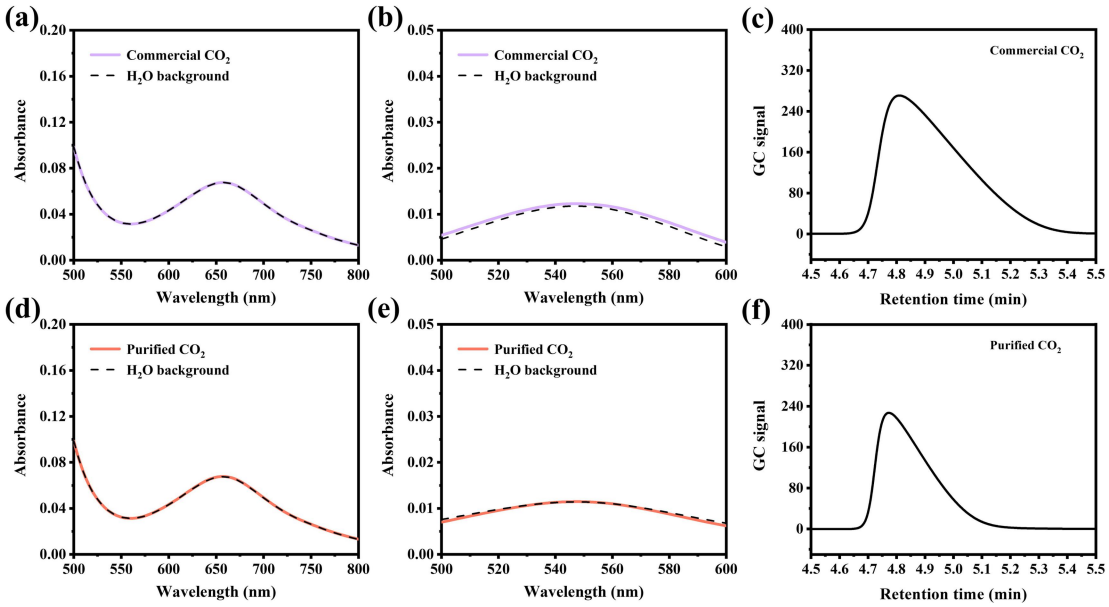


**Fig. S12** | (a, d) The UV-Vis absorption spectra of the deionized water treated by commercial $CO_2$ and purified $CO_2$ using indophenol blue method. (b, e) The UV-Vis absorption spectra of the adsorption liquid using N-(-1-naphthyl)-ethylenediamine dihydrochloride spectrophotometric method. (c, f) Gas chromatography (GC) spectra of commercial $CO_2$ and purified $CO_2$.

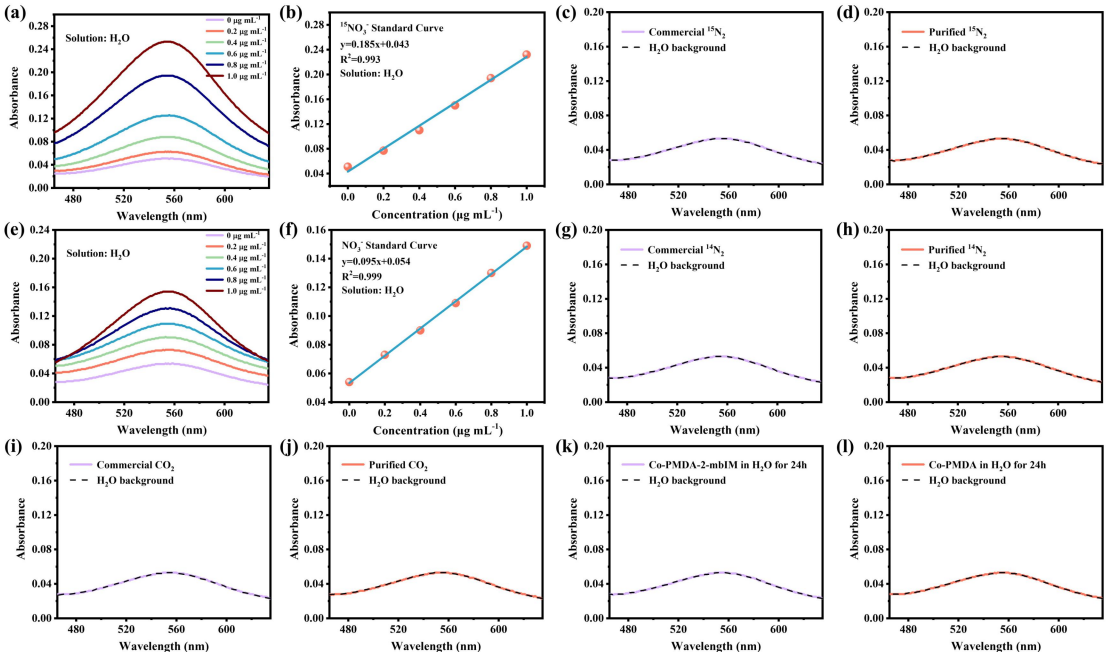


**Fig. S13** | (a-b) The calibration curves for the colorimetric $^{15}NO_3^-$ assay using the modified Griess tests. The UV-Vis absorption spectra of the deionized water treated by (c-d) commercial $^{15}N_2$ and purified $^{15}N_2$; (e-f) The calibration curves for the colorimetric $^{14}NO_3^-$ assay using the modified Griess tests. The UV-Vis absorption spectra of the deionized water treated by (g-h) commercial $^{14}N_2$ and purified $^{14}N_2$ and (i-j) $CO_2$. (k-l) The UV-Vis absorption spectra of Co-PMDA-2-mbIM and Co-PMDA catalysts immersed in $H_2O$ for 24h.

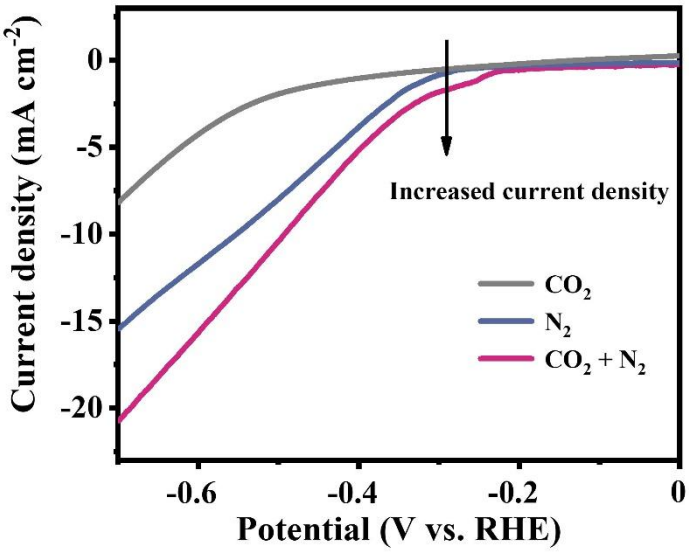


**Fig. S14 |** The linear sweep voltammetry (LSV) of Co-PMDA-2-mbIM catalyst in $CO_2$, $N_2$ and $CO_2$ + $N_2$ saturated electrolyte.

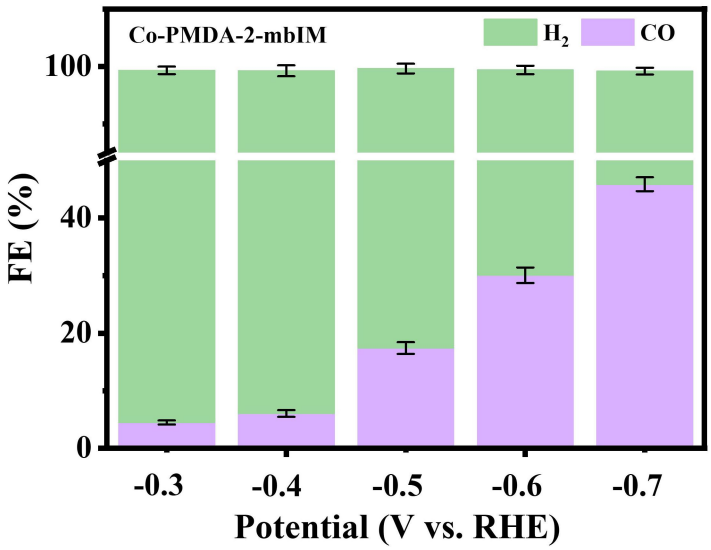


**Fig. S15 |** The product distribution of $CO_2$ reduction reaction for Co-PMDA-2-mbIM catalyst. And Co-PMDA-2mbIM catalyst achieved the FE of up to 48% for converting $CO_2$ into CO.

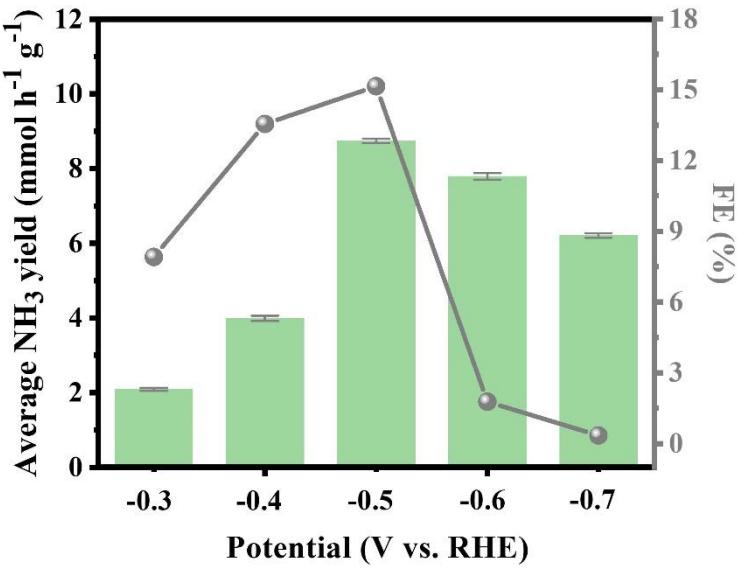


**Fig. S16 |** The $NH_3$ yield rate and Faradaic efficiency of Co-PMDA-2-mbIM catalyst.

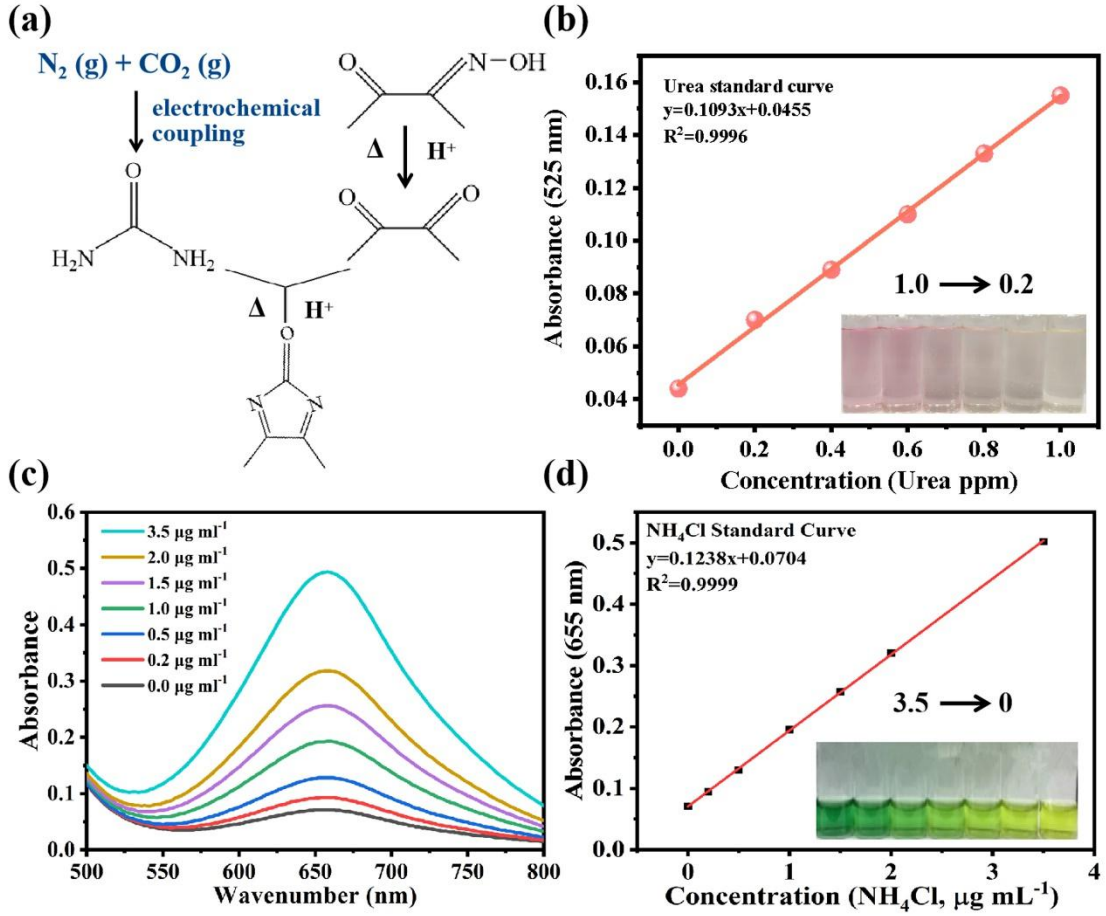


**Fig. S17** | (a) Experimental scheme for the electrochemical synthesis of urea and subsequent determination of the urea concentration generated. Urea detection is based on the diacetyl monoxime method; (b) concentration-absorbance of urea solution with a series of standard concentration (0.2-1.0 μg $mL^{-1}$) in 0.1 M $KHCO_3$. The absorbance at 525 nm was measured by UV-vis spectrophotometer. The standard curve shown good linear relation of absorbance with urea concentration (y=0.1093x+0.0455, $R^2$=0.9996); (c) UV-vis curves and (d) concentration-absorbance of $NH_4Cl$ solution with a series of standard concentration (0-3.5 μg $mL^{-1}$) in 0.1 M $KHCO_3$. The absorbance at 655 nm was measured by UV-vis spectrophotometer. The standard curve shown good linear relation of absorbance with $NH_4Cl$ concentration (y=0.1238x+0.0704, $R^2$=0.9999).

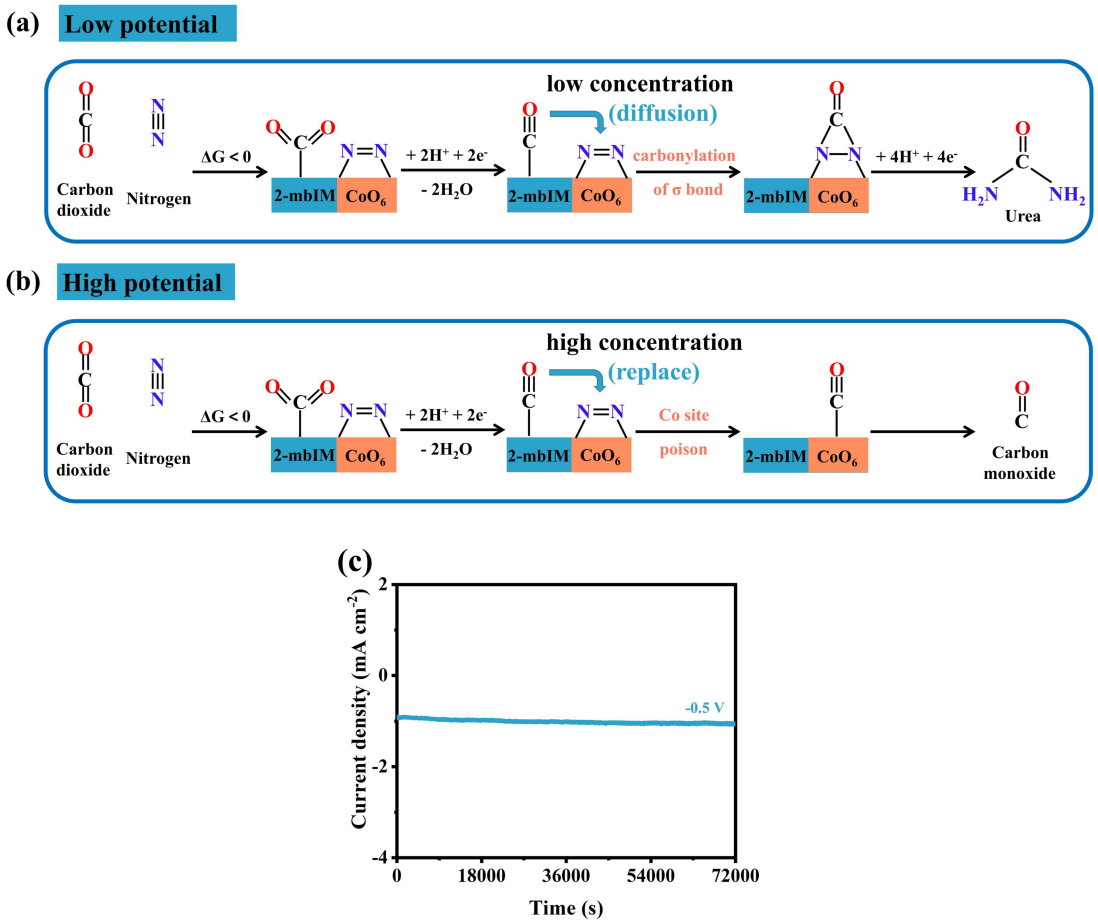


**Fig. S18** | The host-guest interaction in Co-PMDA-2-mbIM participates in the urea electrosynthesis reaction at (a) low potential and (b) high potential. The chronamperometric curves of Co-PMDA-2-mbIM at -0.5 V vs. RHE for 20 h in $N_2$ + $CO_2$-saturated in 0.1 M $KHCO_3$ solution.

Regarding the Co-PMDA-2-mbIM sample, the peaks in the $N_2$-TPD spectrum display the enhanced peak intensity and appear at higher temperatures by contrast to the $CO_2$-TPD results (**Fig. 4g-h**), evidencing that $N_2$ can be preferentially adsorbed on the catalyst surface than that of $CO_2$. As shown in **Fig. 18a-b**, $N_2$ and $CO_2$ will be specifically adsorbed and activated on the electrophilic $CoO_6$ region and nucleophilic 2-mbIM region successively. At low potentials, CO generated from the $CO_2$ reduction reaction easily diffuses to *N=N* intermediates and realizes C-N bond coupling via σ orbital carbonylation strategy (**Fig. S18a**). However, when the potential is shifted below -0.5 V vs. RHE, Co-PMDA-2-mbIM exhibits the increased FE of CO at high potential (**Fig. 4c**). It has been reported that high concentrations of CO readily poison metal active sites [*Nat Commun*., **2021**, *12*, 3342; *PNAS*., **2021**, *118*, e2107332118]. As shown in **Fig. S18b**, the excessively released CO will replace the *N=N*

intermediates and poison the Co sites of the electrophilic $CoO_6$ region, thus prevent the proceeding of C-N coupling reaction, resulting in the decrease of urea electrosynthesis performance.

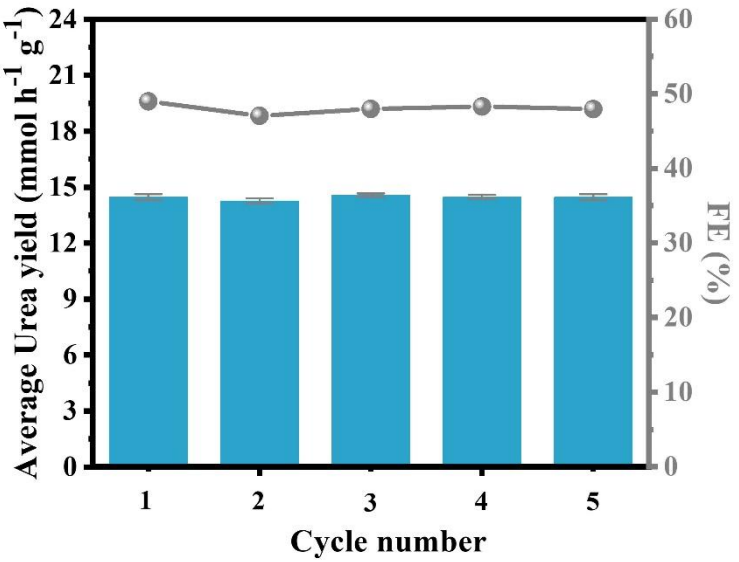


**Fig. S19 |** The Faradaic efficiency and urea production rate of Co-PMDA-2-mbIM catalyst at -0.5 V vs. RHE during recycling tests for five times.

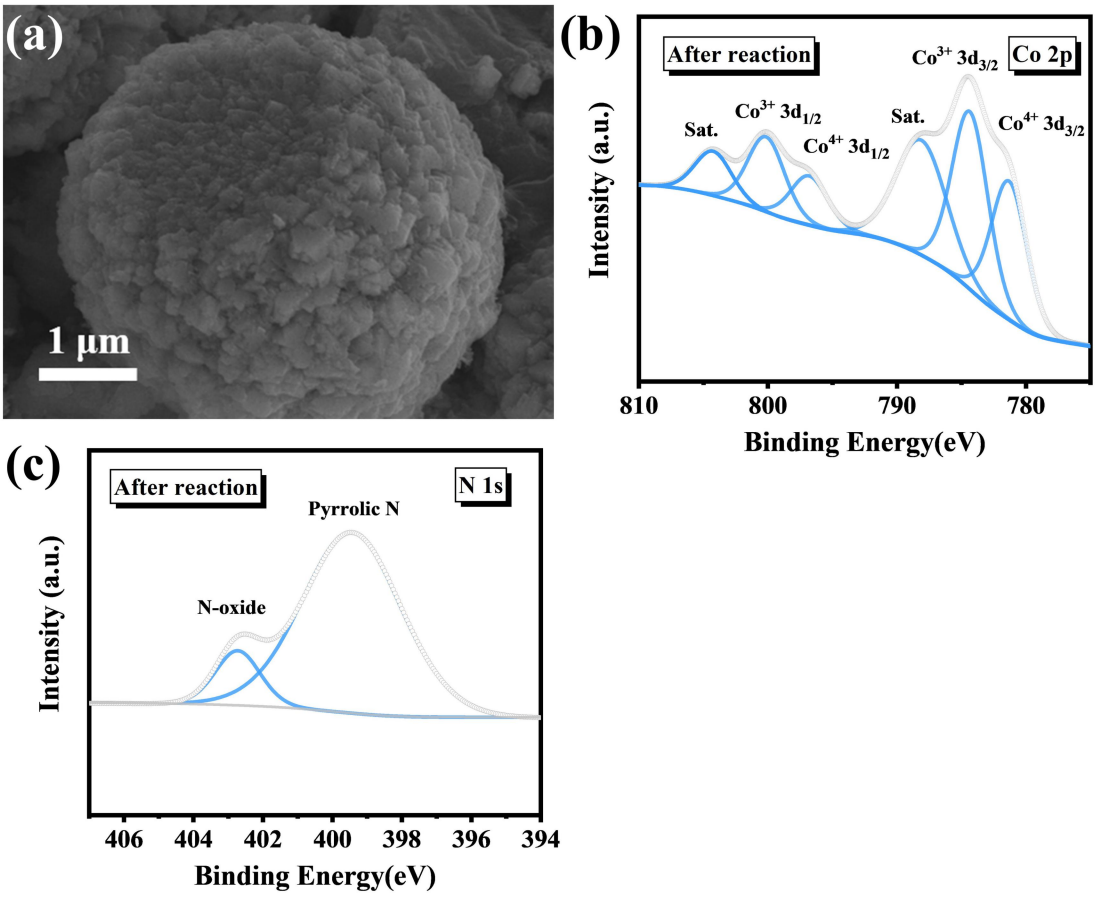


**Fig. S20 |** (a) SEM image; (b) high-resolution Co 2p spectrum and (c) N 1s spectrum of Co-PMDA-2-mbIM catalyst after 20 h electrolysis.

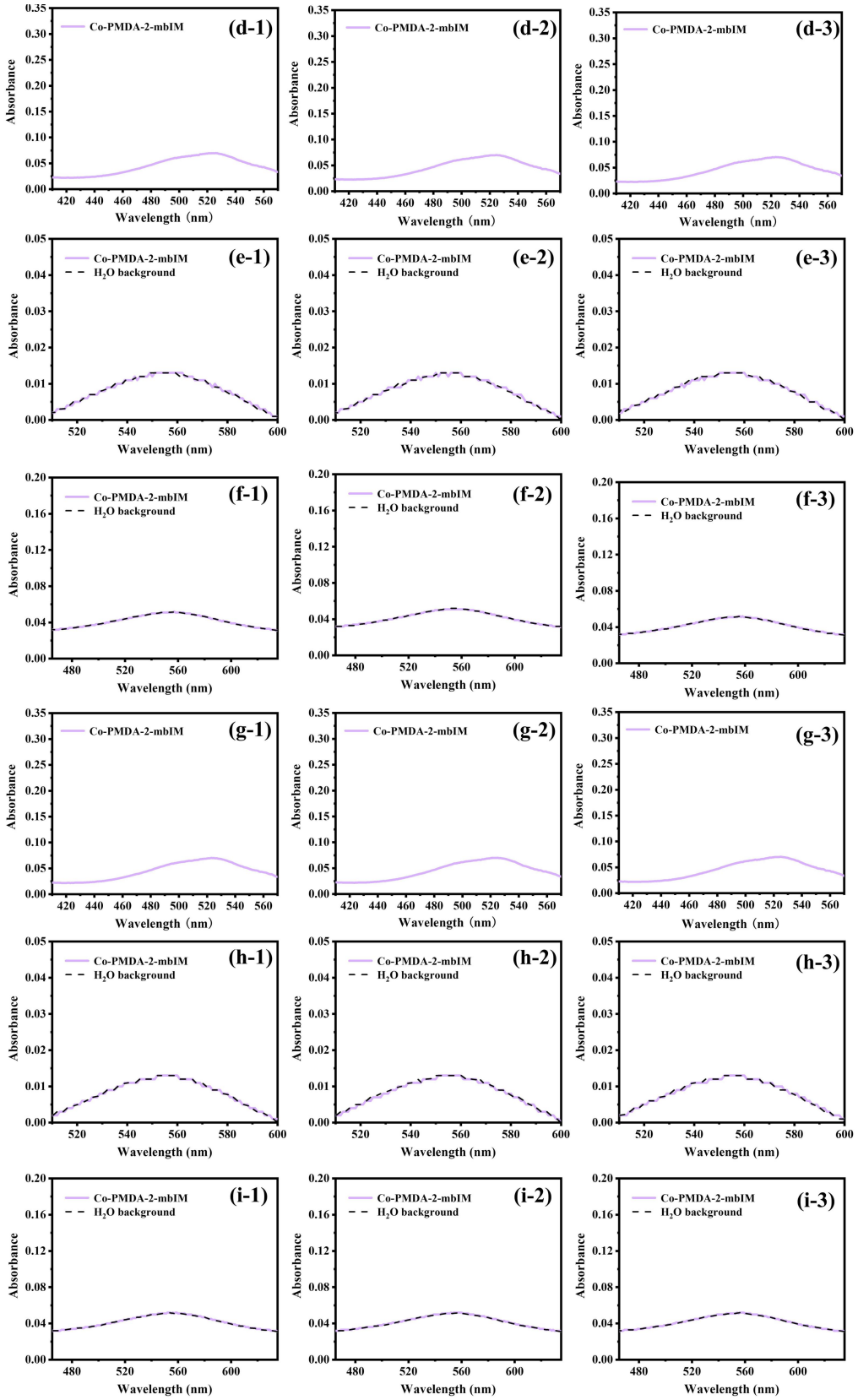


**Fig. S20 |** The UV-Vis absorption spectra the (d) $^{14}$urea, (e) $^{14}NO_2^-$, (f) $^{14}NO_3^-$, (g) $^{15}$urea, (h) $^{15}NO_2^-$ and (i) $^{15}NO_3^-$ catalyzed by the Co-PMDA-2-mbIM catalysts with a small and fixed volume of $^{14}N_2$+$CO_2$ and $^{15}N_2$+$CO_2$ gas.

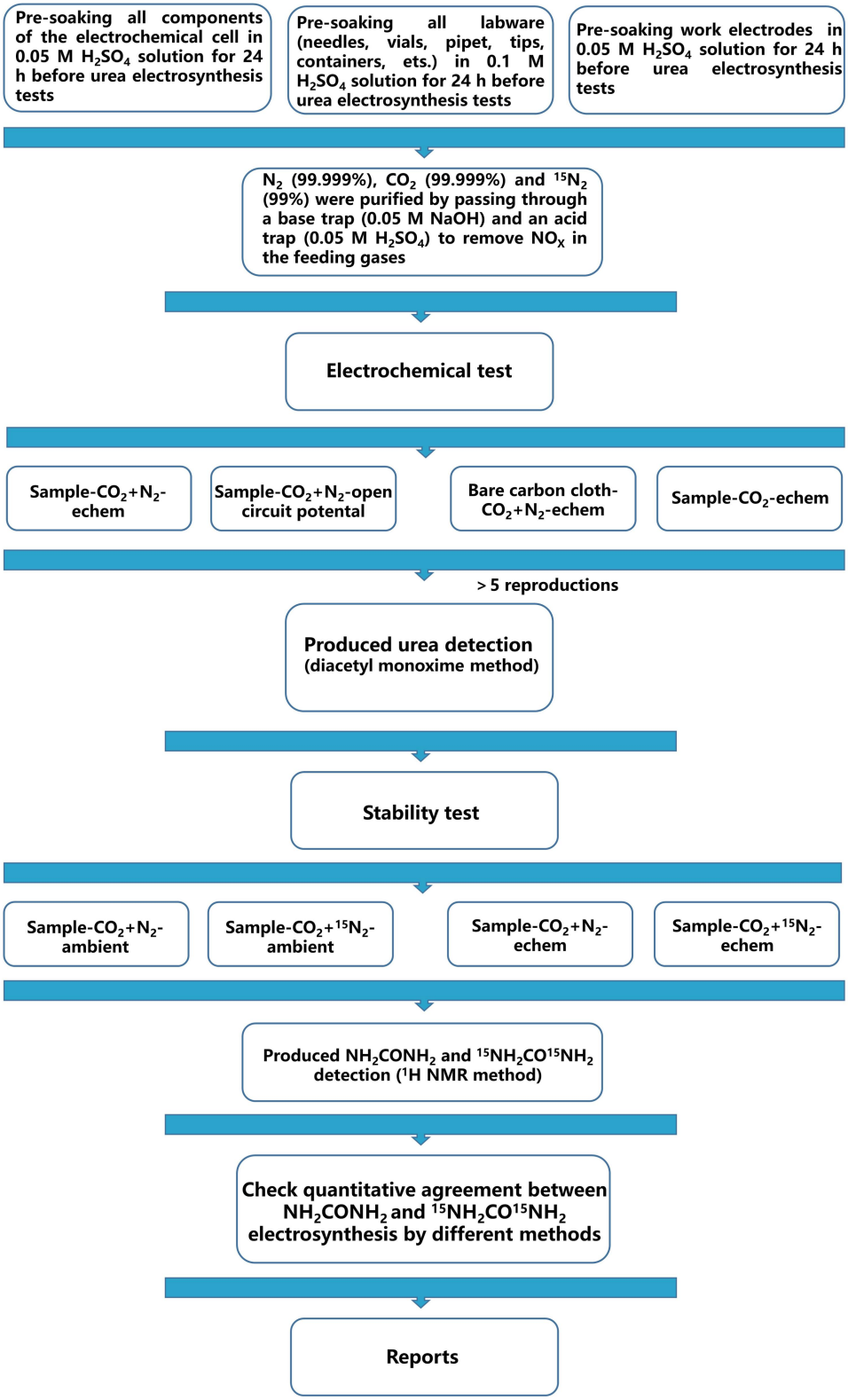


**Scheme S1 |** The urea electrosynthesis experimental produces utilized in this work.

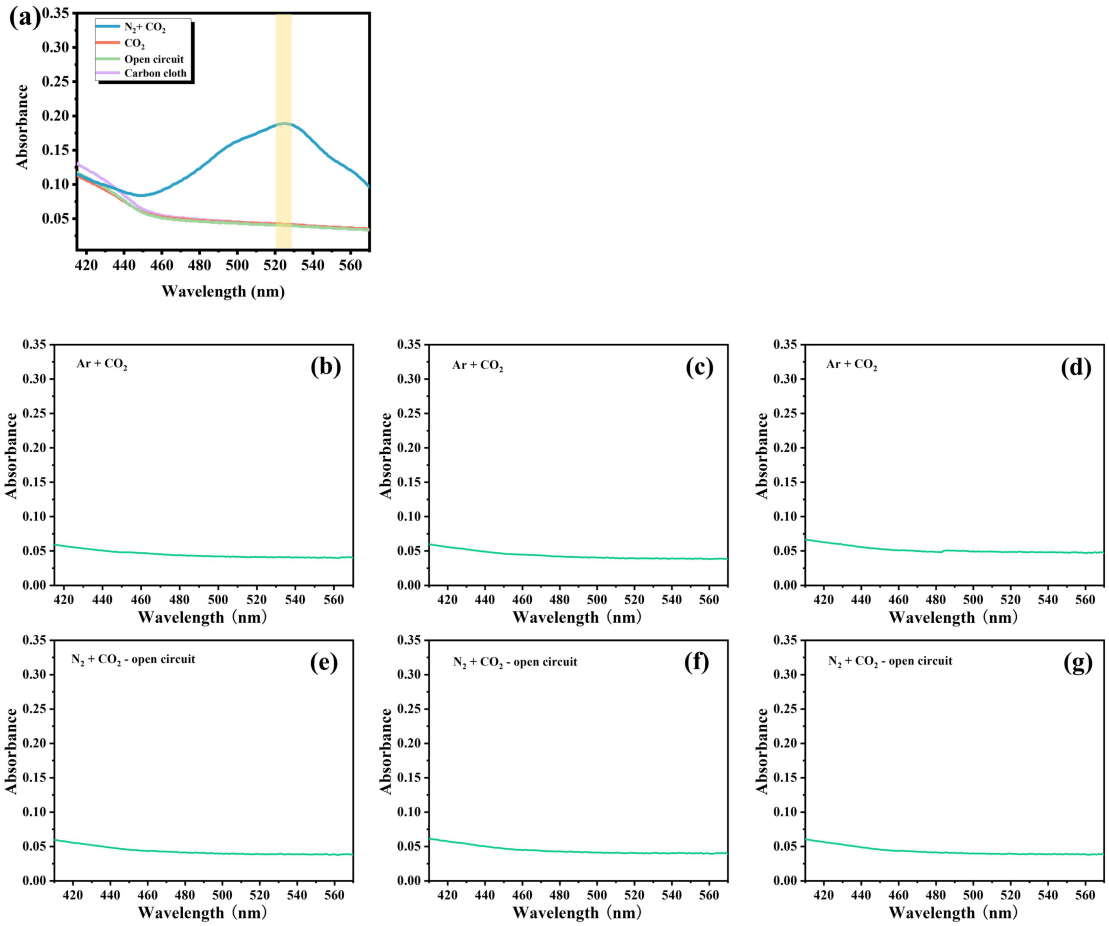


**Fig. S21** | (a) UV-vis spectra of the electrolyte stained with diacetyl monoxime indicator for the bare carbon cloth electrolysis 2h in $N_2$+$CO_2$-saturated solution, without and after 2h electrolysis at the potential of -0.5 V in $N_2$+$CO_2$-saturated solution, electrolysis 2h in $CO_2$-saturated solution; the UV-Vis absorption spectra of the electrolyte solution that electrolysis under (b-d) Ar+$CO_2$ and (e-g) $N_2$+$CO_2$ without any applied potential for three times.

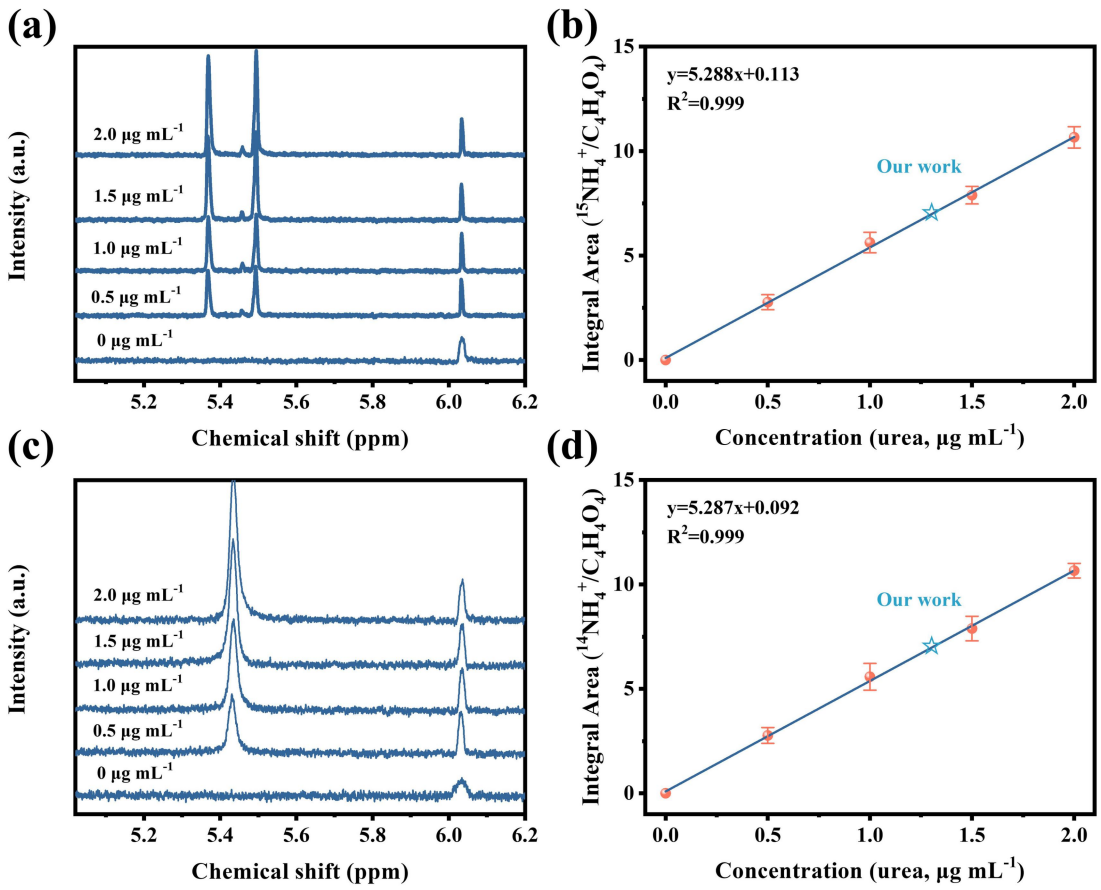


**Fig. S22 |** (a) $^{1}H$ NMR spectra of standard $^{15}NH_2CO^{15}NH_2$ solution with various concentrations of 0.5-2.0 μg $mL^{-1}$; (b) integral area ($^{15}NH_2CO^{15}NH_2$ / $C_4H_4O_4$) - concentration linear relation calibrated using standard $^{15}NH_2CO^{15}NH_2$ solution. (c) $^{1}H$ NMR spectra of standard $^{14}NH_2CO^{14}NH_2$ solution with various concentrations of 0.5-2.0 μg $mL^{-1}$; (d) integral area ($^{14}NH_2CO^{14}NH_2$ / $C_4H_4O_4$) - concentration linear relation calibrated using standard $^{14}NH_2CO^{14}NH_2$ solution.

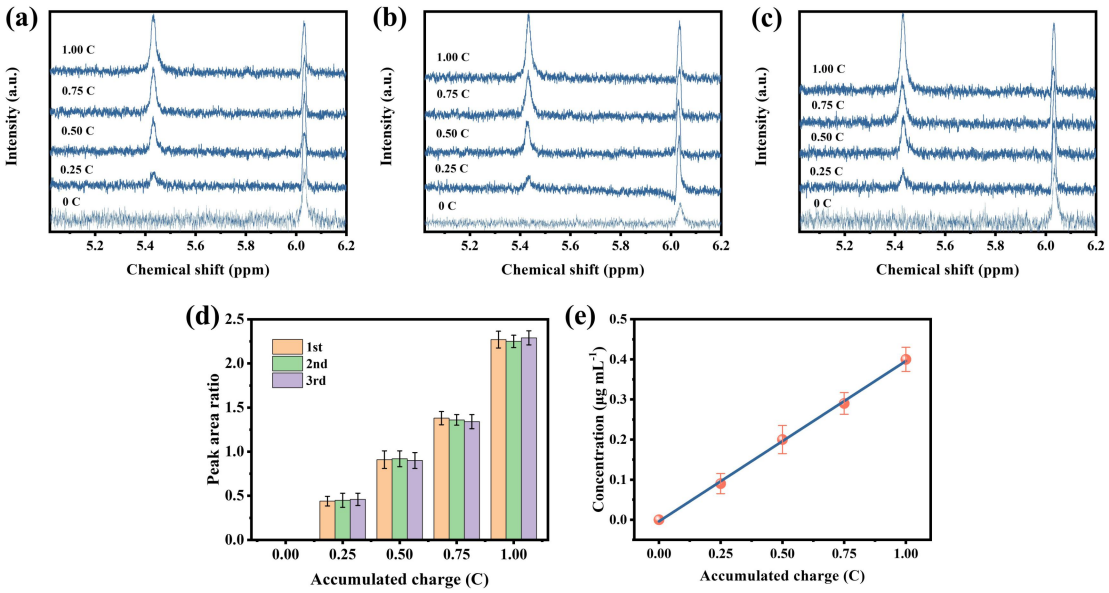


**Fig. S23** | (a-c) $^{1}$H NMR spectra of $^{14}NH_2CO^{14}NH_2$ from all three $^{14}N_2$ and $CO_2$ reduction experiments as a function of charge passed. (d) The integral area ratio ($^{14}NH_2CO^{14}NH_2$ / $C_4H_4O_4$) from all three independent tests as a function of charge passed. (e) The average concentration of $^{14}NH_2CO^{14}NH_2$ as measured by NMR from the $^{14}N_2$ and $CO_2$ reduction experiments as a function of charge passed.

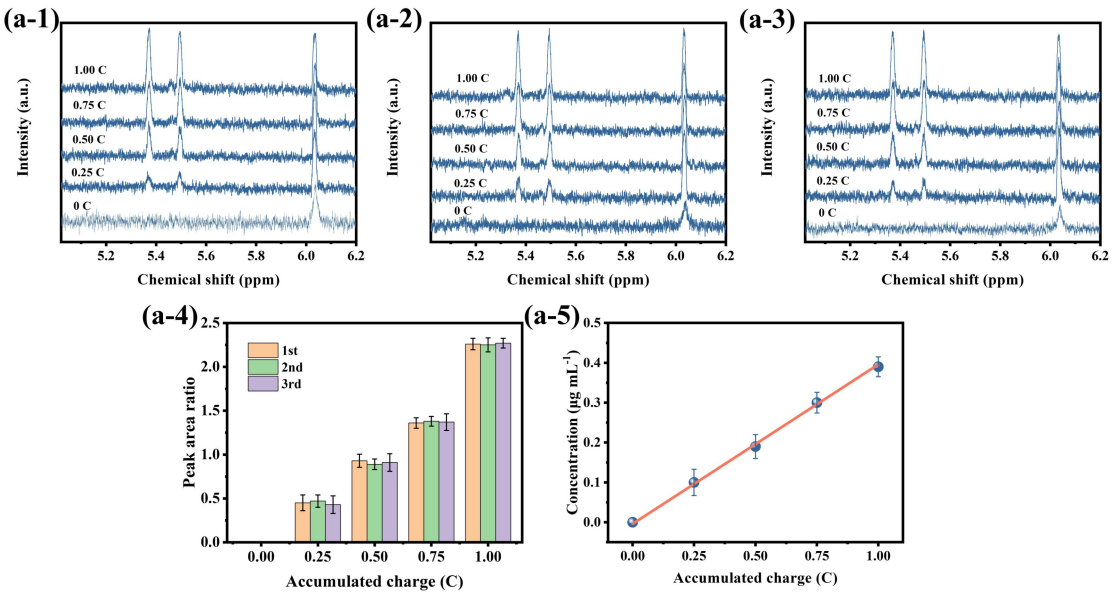


**Fig. S24 |** (a-1~a-3) $^{1}H$ NMR spectra of $^{15}NH_2CO^{15}NH_2$ from all three $^{15}N_2$ and $CO_2$ reduction experiments (-0.5 V vs. RHE) as a function of charge passed. (a-4) The integral area ratio ($^{15}NH_2CO^{15}NH_2$ / $C_4H_4O_4$) from all three independent tests as a function of charge passed. (a-5) The average concentration of $^{15}NH_2CO^{15}NH_2$ as measured by NMR from the $^{15}N_2$ and $CO_2$ reduction experiments as a function of charge passed.

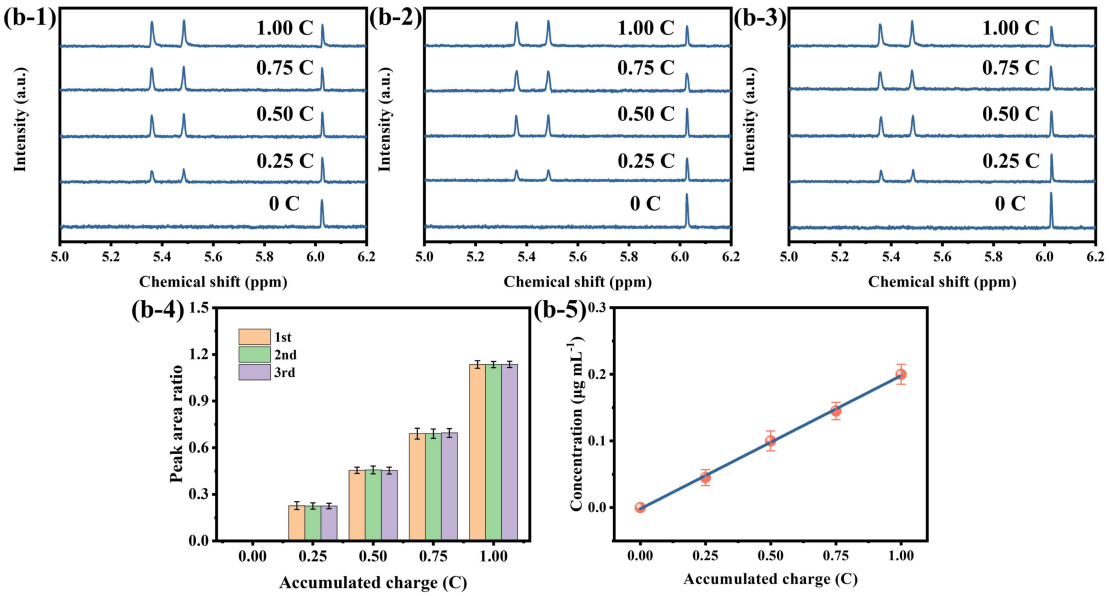


**Fig. S24 |** (b-1~b-3) $^{1}$H NMR spectra of $^{15}NH_2CO^{15}NH_2$ from all three $^{15}N_2$ and $CO_2$ reduction experiments (-0.4 V vs. RHE) as a function of charge passed. (b-4) The integral area ratio ($^{15}NH_2CO^{15}NH_2$ / $C_4H_4O_4$) from all three independent tests as a function of charge passed. (b-5) The average concentration of $^{15}NH_2CO^{15}NH_2$ as measured by NMR from the $^{15}N_2$ and $CO_2$ reduction experiments as a function of charge passed.

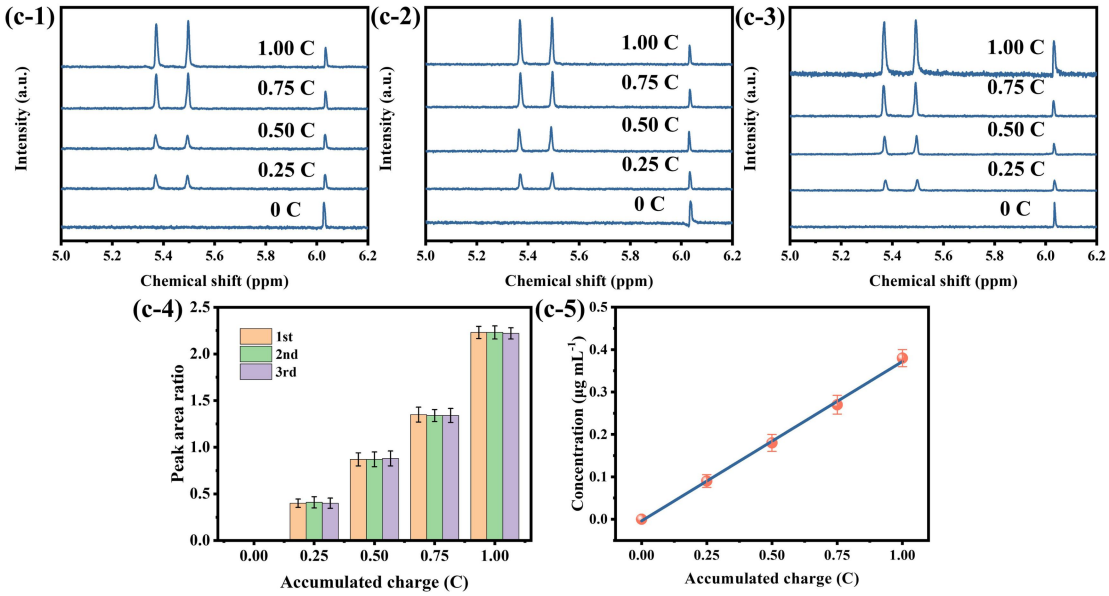


**Fig. S24 |** (c-1~c-3) $^{1}H$ NMR spectra of $^{15}NH_2CO^{15}NH_2$ from all three $^{15}N_2$ and $CO_2$ reduction experiments (-0.6 V vs. RHE) as a function of charge passed. (c-4) The integral area ratio ($^{15}NH_2CO^{15}NH_2$ / $C_4H_4O_4$) from all three independent tests as a function of charge passed. (c-5) The average concentration of $^{15}NH_2CO^{15}NH_2$ as measured by NMR from the $^{15}N_2$ and $CO_2$ reduction experiments as a function of charge passed.

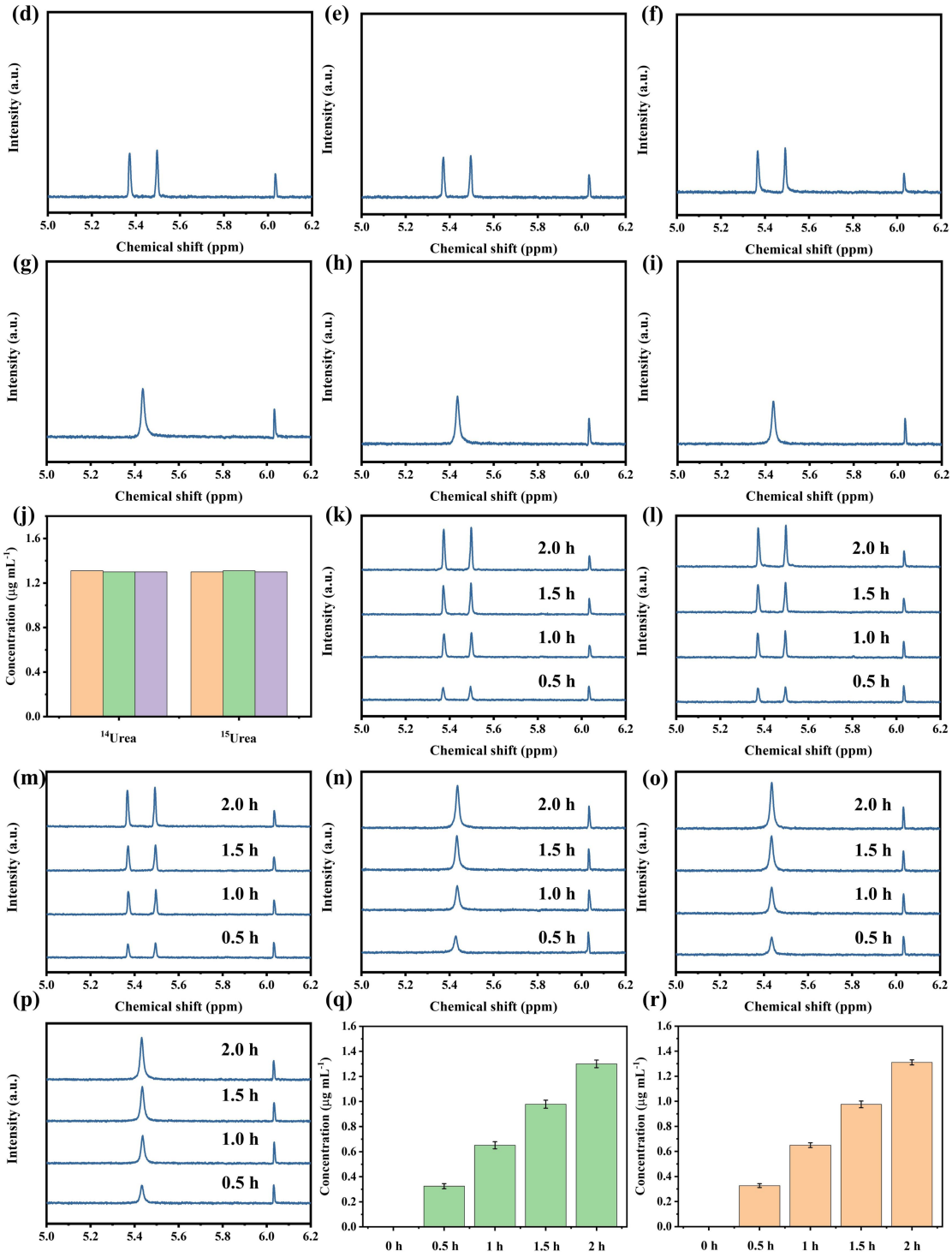


**Fig. S24 |** The $^{1}$H NMR spectra of (d-f) $^{15}$urea and (g-i) $^{14}$urea catalyzed at -0.5 V vs. RHE by the Co-PMDA-2-mbIM catalyst; (j) The quantitative agreement of the concentration of $^{15}$urea and $^{14}$urea. The $^{1}$H NMR spectra of (k-m) $^{15}$urea and (n-p) $^{14}$urea catalyzed at different time-point. The concentration of (q) $^{15}$urea and (r) $^{14}$urea at different time-point.

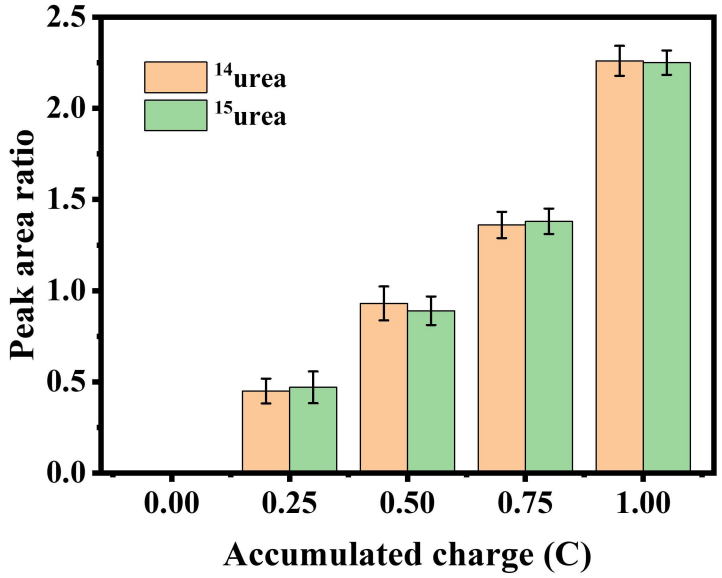


**Fig. S25 |** Comparison of the average concentration of $^{14}NH_2CO^{14}NH_2$ and $^{15}NH_2CO^{15}NH_2$, as measured by NMR, from the $^{14}N_2$ (or $^{15}N_2$) and $CO_2$ reduction experiments, respectively, as a function of charge passed.

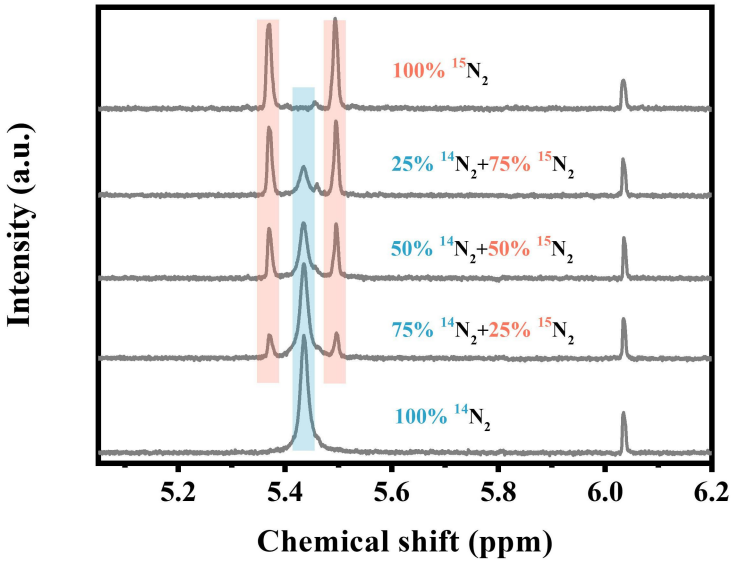


**Fig. S26 |** The impact of $^{14}N_2$ and $^{15}N_2$ gas mixture (100% $^{14}N_2$, 25%/75% $^{14/15}N_2$, 50%/50% $^{14/15}N_2$, 75%/25% $^{14/15}N_2$, 100% $^{15}N_2$) on the isotopic distribution of the produced urea by $^{1}$H-NMR spectrometry.

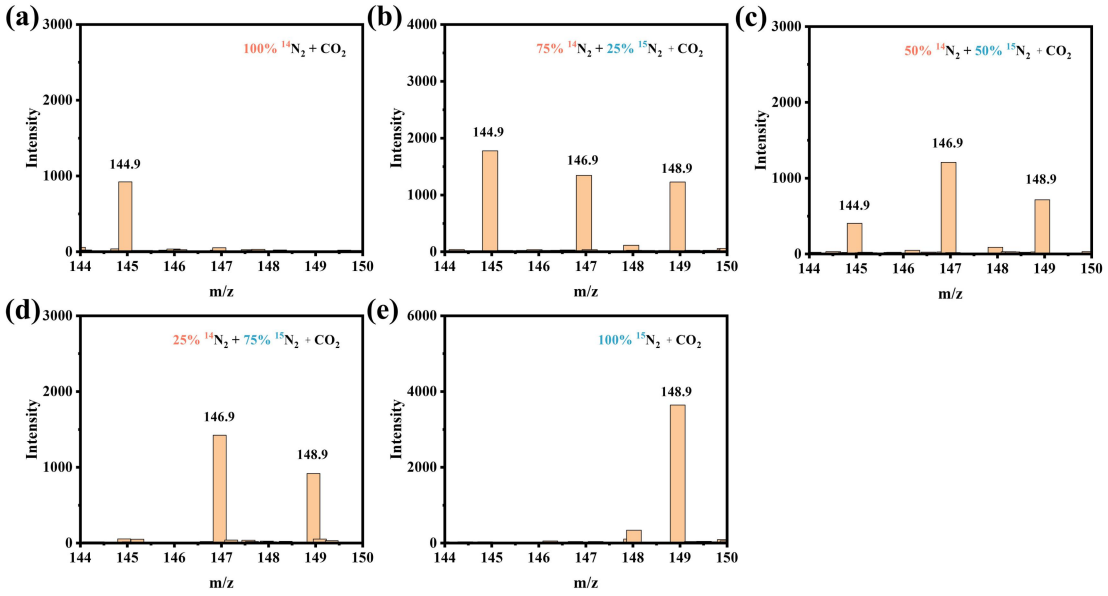


**Fig. S27** | The impact of $^{14}N_2$ and $^{15}N_2$ gas mixture (100% $^{14}N_2$, 25%/75% $^{14/15}N_2$, 50%/50% $^{14/15}N_2$, 75%/25% $^{14/15}N_2$, 100% $^{15}N_2$) on the isotopic distribution of the produced urea by mass spectrometry.

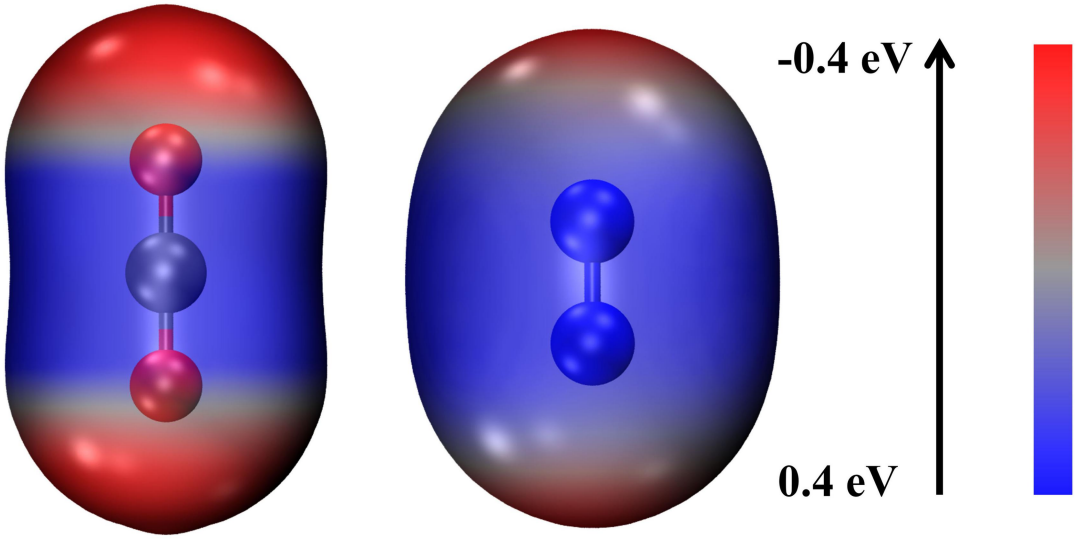


**Fig. S28 |** Electron-density isosurface of $CO_2$ molecule (left) and $N_2$ molecule (right), the color bar represents the electrostatic potential scale.

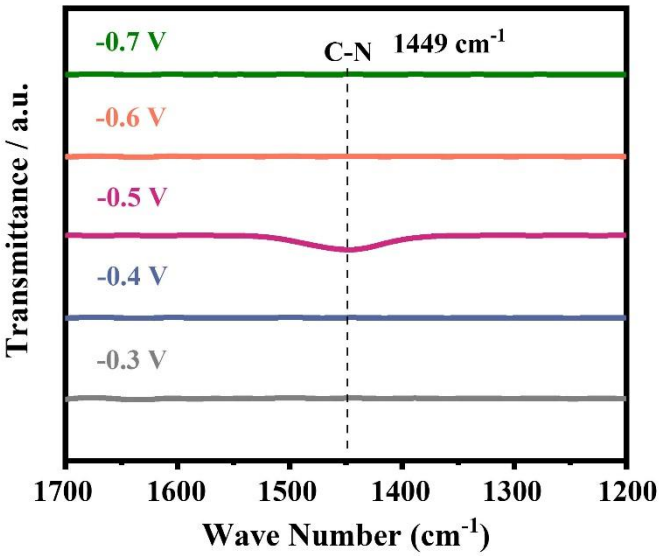


**Fig. S29 |** The FTIR spectroscopy of Co-PMDA monitored at each given potential.

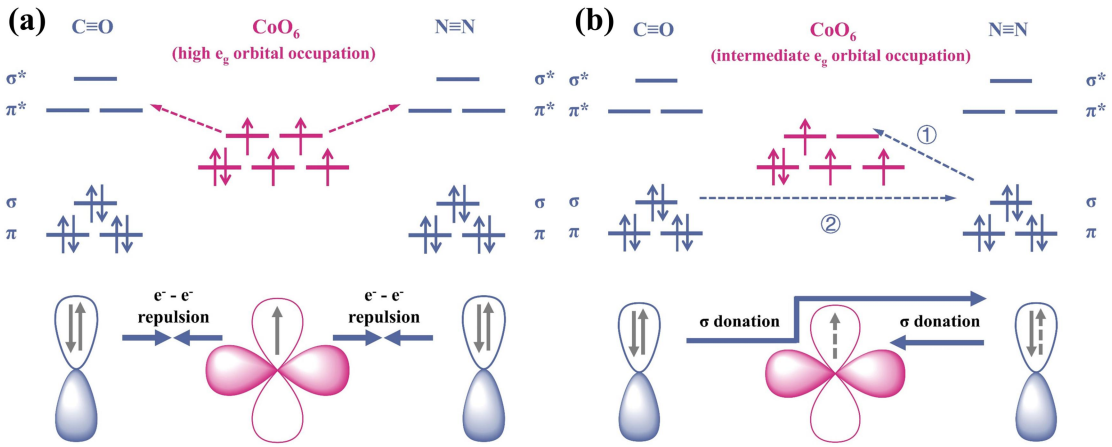


**Scheme S2 |** (a) The high $e_g$ orbital occupied $CoO_6$ and (b) the intermediate $e_g$ orbital occupied $CoO_6$ participated electrocatalytic C-N coupling reaction during urea electrosynthesis.

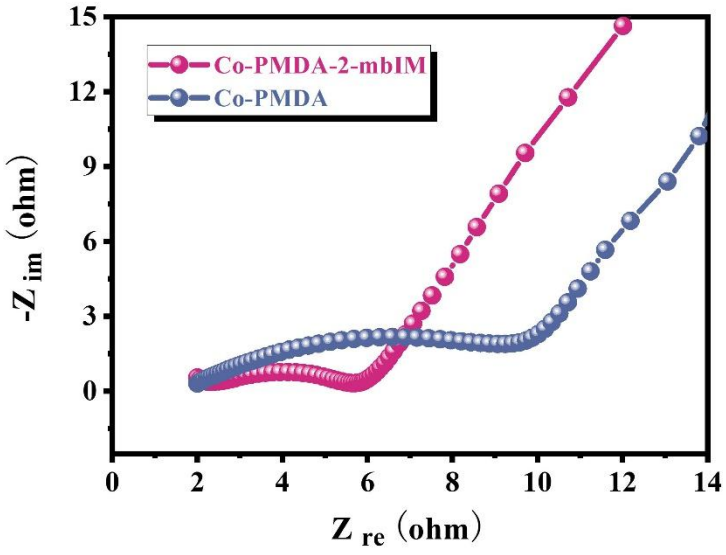


**Fig. S30 |** The EIS spectrum of Co-PMDA and Co-PMDA-2-mbIM catalysts.

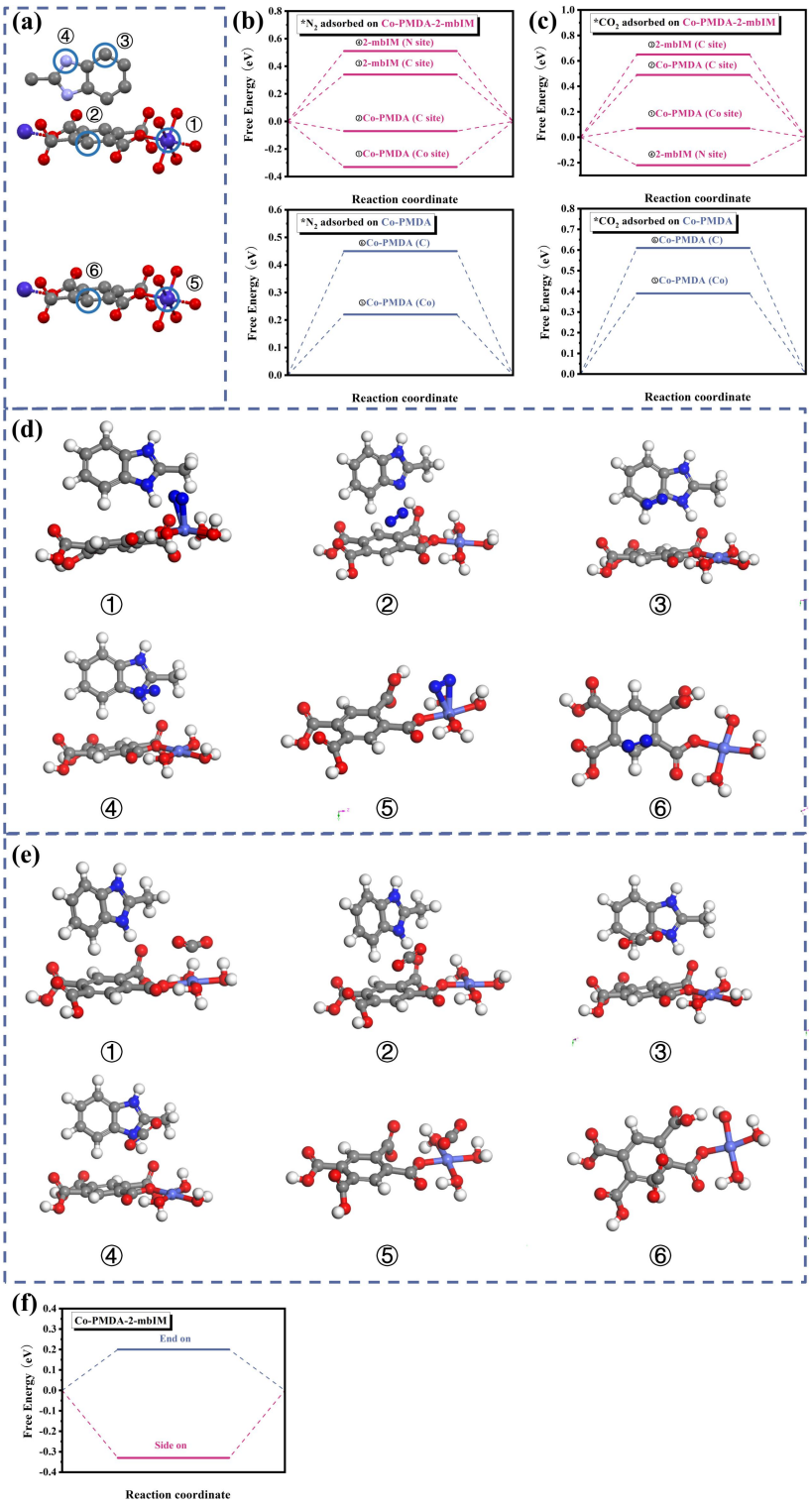


**Fig. S31 |** (a) The active sites in Co-PMDA-2-mbIM and Co-PMDA catalysts for $N_2$ and $CO_2$ adsorption; free energy diagrams for (b) $N_2$ and (c) $CO_2$ adsorption on Co-PMDA and Co-PMDA-2-mbIM catalysts; the optimized geometry of (d) $N_2$ and (e) $CO_2$ adsorbed on Co-PMDA and Co-PMDA-2-mbIM catalysts. (f) $N_2$ adsorbed on the Co-PMDA-2-mbIM catalyst by different configurations.

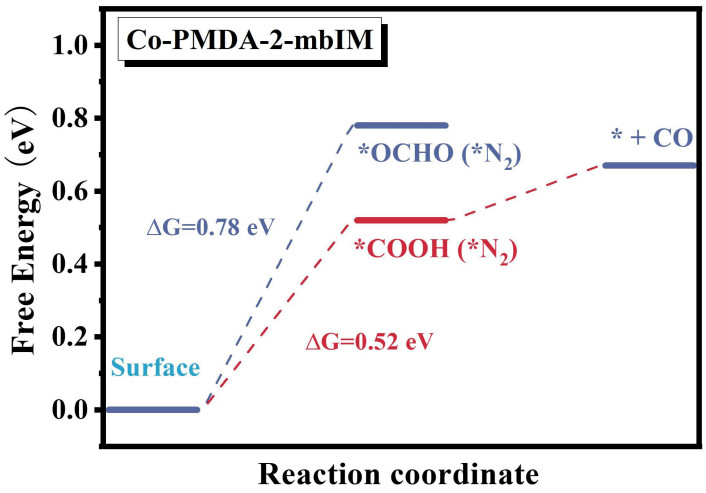


**Fig. S32 |** Free energy diagram for *COOH and *OCHO intermediates.

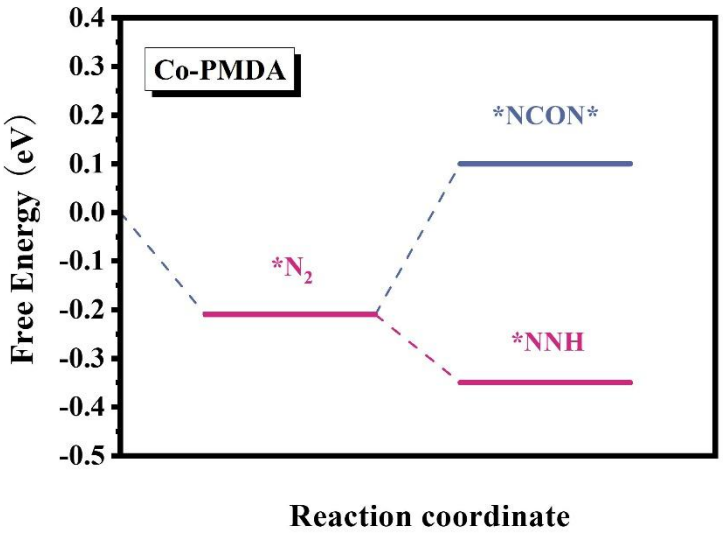


**Fig. S33 |** The free energy diagrams for $N_2$ adsorption and further activation on the Co-PMDA catalyst.

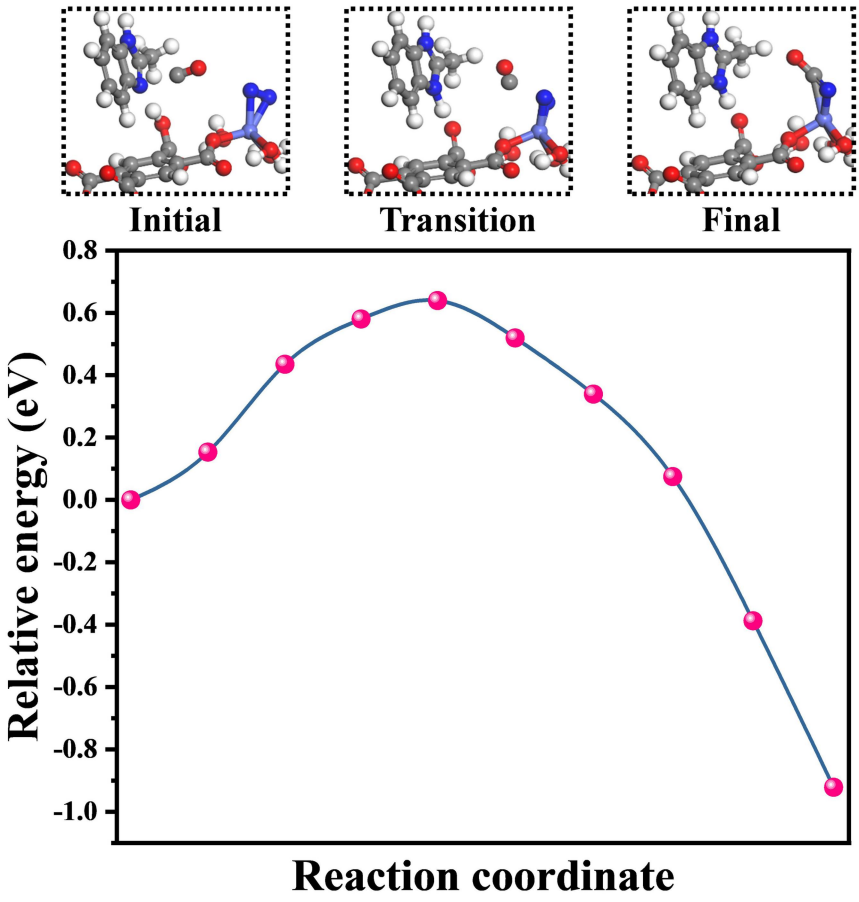


**Fig. S34 |** The reaction pathway of *$N_2$ and *CO coupling into *NCON*. The structures of the initial, transition and final states along with the *NCON* formation are also presented.

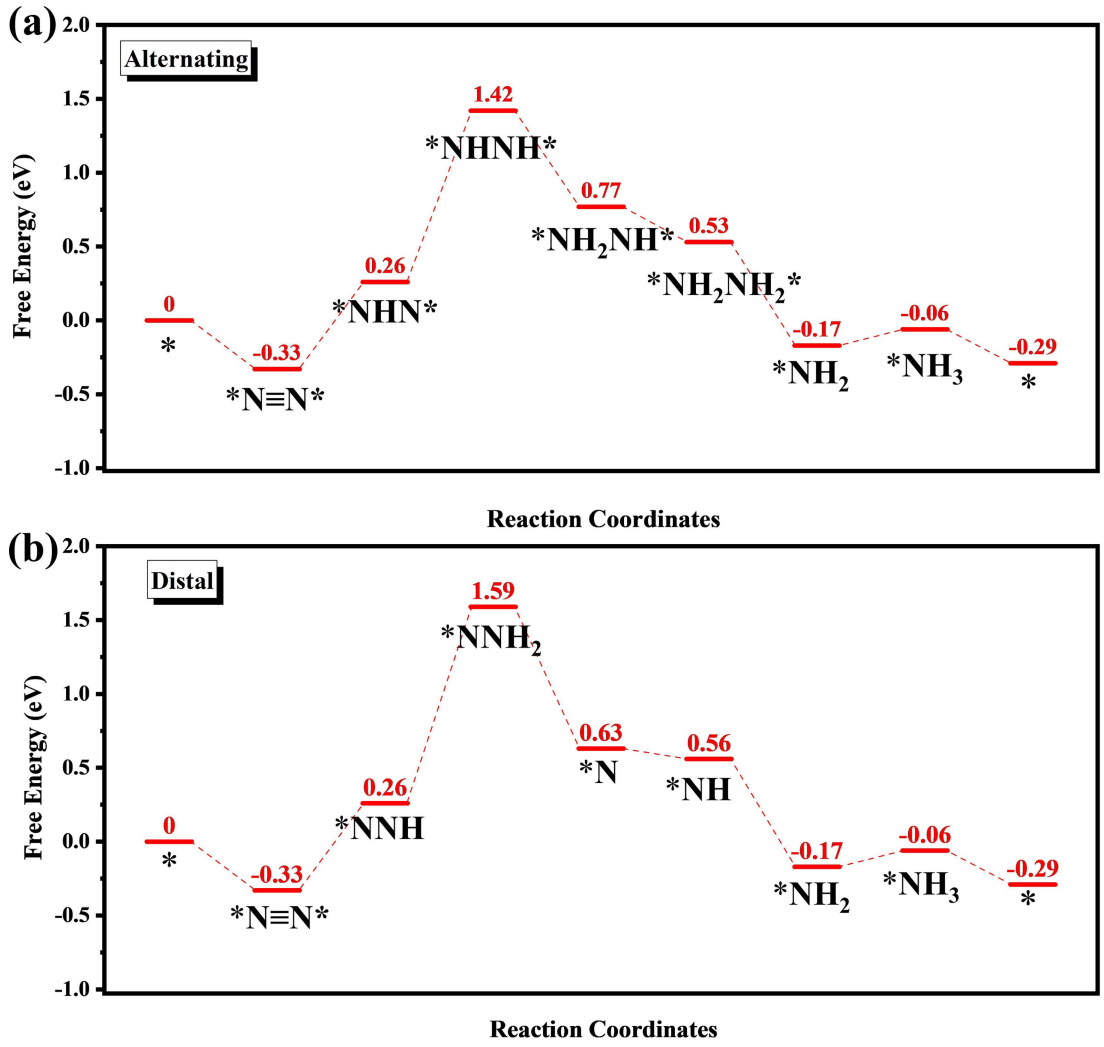


**Fig. S35 |** The free energy diagrams for $N_2$ adsorption and further activation on the Co-PMDA-2-mbIM catalyst.

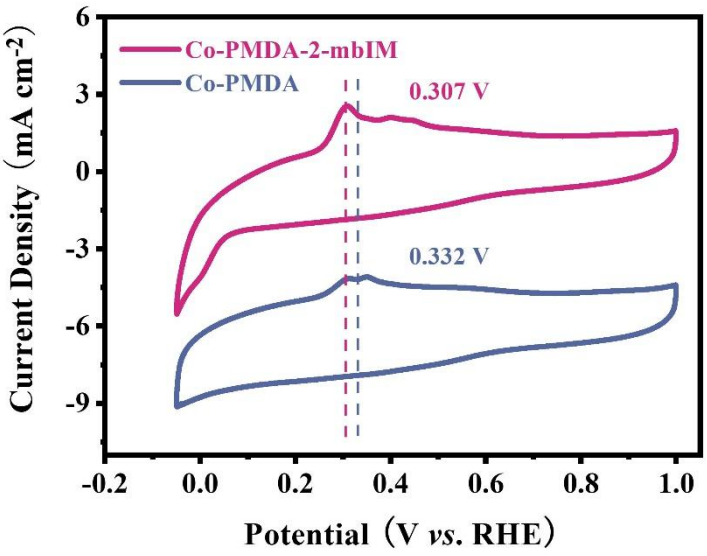


**Fig. S36** | CO-stripping measurements of Co-PMDA and Co-PMDA-2-mbIM catalysts.

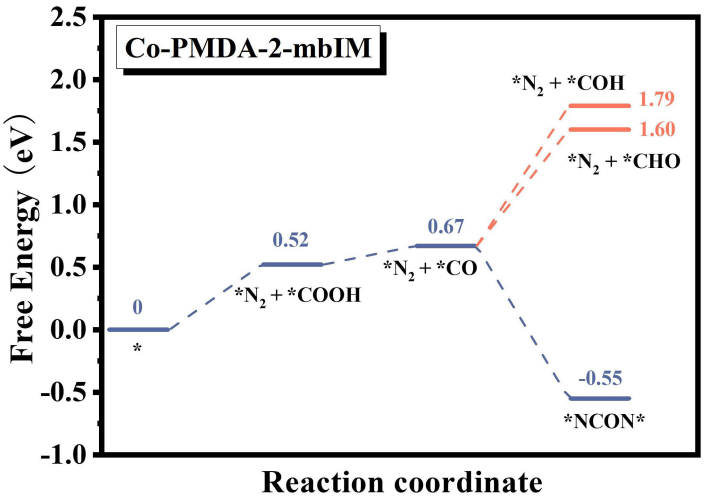


**Fig. S37 |** Free energy diagram for *COH and *CHO intermediates.

| MOF | Co-PMDA-2-mbIM |
|---|---|
| Empirical formula | $C_{26}H_{28}CoN_4O_{12}$ |
| Formula weight | 647.45 |
| Temperature/K | 291 |
| Crystal system | triclinic |
| Space group | P-1 |
| a/Å | 7.0903 |
| b/Å | 9.6953 |
| c/Å | 10.7313 |
| α/° | 93.062 |
| β/° | 104.142 |
| γ/° | 107.964 |
| Volume/Å$^3$ | 673.80 |
| Z | 1 |
| $\rho_{calc}$ g/cm$^3$ | 1.596 |
| μ/mm$^{-1}$ | 0.71073 |
| F(000) | 335 |
| Crystal size/mm$^3$ | 0.31 × 0.26 × 0.24 |
| 2θ range for data collection/° | 3.141 to 25.999 |
| Index ranges | $-8 \leq h \leq 8$ |
| | $-11 \leq k \leq 11$ |
| | $-13 \leq l \leq 13$ |
| Reflections collected | 10858 |
| Independent reflections | 2602 |
| | [$R_{int}$ = 0.0232, $R_{sigma}$ = 0.0135] |
| Goodness-of-fit on $F^2$ | 1.022 |
| Final R indexes [I >= 2σ (I)] | $R^1$= 0.0249, $wR^2$ = 0.0720 |
| Final R indexes [all data] | $R^1$= 0.0250, $wR^2$ = 0.0719 |
| Data/restraints/parameters | 2602/1/197 |

**Table S1 |** The crystal data and structure refinements of Co-PMDA-2-mbIM catalyst.

| | HS (%) | LS (%) | $e_g$ electron filling | Spin state type |
|---|---|---|---|---|
| Co-PMDA | 97.99 | 2.01 | 1.96 | HS |
| Co-PMDA-2-mbIM | 41.61 | 58.39 | 1.04 | IS |

**Table S2 |** The $e_g$ occupation of Co-PMDA and Co-PMDA-2-mbIM with different spin state.

| Gas | Flow rate (sccm) | Purging time (min) | Volume of gas used (mL) | $NH_3^*$ (ng $mL^{-1}$) | $NO_x^*$ (ng $mL^{-1}$) | $N_2O$ (ppm) |
|---|---|---|---|---|---|---|
| Commercial $^{14}N_2$ | 30 | 720 | 21600 | 2.24# | 11.43 | 0.05# |
| Purified $^{14}N_2$ | | | | 2.24# | 6.32# | 0.05# |
| Commercial $CO_2$ | 30 | 720 | 21600 | 2.24# | 14.29 | 0.05# |
| Purified $CO_2$ | | | | 2.24# | 6.32# | 0.05# |

*The concentrations of NOx and $NH_3$ were calculated based on 80 mL electrolyte.
#For the contaminants that were not detected, their corresponding concentration was assumed to be equal to the related limit of detection.

**Table S3 |** Concentration of potential $NH_3$, NOx and $N_2O$ contaminants supplied in 12h experiments using different feed gas.

| Catalysts | Electrolyte | Potential (V vs. RHE) | Faradaic efficiency | Urea yield rate | Reference |
|---|---|---|---|---|---|
| Co-PMDA-2-mbIM | 0.1 M $KHCO_3$ | -0.5 V | 48.97 % | 14.47 mmol $h^{-1}$ $g^{-1}$ | This work |
| $Pd_1Cu_1/TiO_2$-400 | 0.1 M $KHCO_3$ | -0.4 V | 8.92 % | 3.36 mmol $h^{-1}$ $g^{-1}$ | Nat Chem., 2020, 12, 717-724 |
| Bi-$BiVO_4$ hybrids | 0.1 M $KHCO_3$ | -0.4 V | 12.55 % | 5.91 mmol $h^{-1}$ $g^{-1}$ | Angew Chem Int Ed., 2021, 60, 10910-10918 |
| $BiFeO_3/BiVO_4$ hybrids | 0.1 M $KHCO_3$ | -0.4 V | 17.18 % | 4.94 mmol $h^{-1}$ $g^{-1}$ | Chem Sci., 2021, 12, 6048 |
| Te-Pd nanocrystal | 0.1 M $KHCO_3$ + 0.01 M $KNO_2$ | -1.1 V | 12.2 % | -- | Nano Lett., 2020, 20, 8282-8289 |

**Table S4 |** Comparison of the electrocatalytic activity of Co-PMDA-2-mbIM catalyst to produce urea through urea electrosynthesis with previously reported urea electrosynthesis catalysts.